University of Groningen

The origin of the dust in high-redshift quasars

Valiante, Rosa; Schneider, Raffaella; Salvadori, Stefania; Bianchi, Simone

IMPORTANT NOTE: You are advised to consult the publisher's version (publisher's PDF) if you wish to cite from it. Please check the document version below.

Document Version
Publisher's PDF, also known as Version of record

Publication date:
2011

Link to publication in University of Groningen/UMCG research database

The origin of the dust in high-redshift quasars: the case of SDSS J1148+5251

Rosa Valiante,[1,2]★ Raffaella Schneider,[3] Stefania Salvadori[4] and Simone Bianchi[2]

[1]*Dipartimento di Astronomia, Universita' di Firenze, Largo Enrico Fermi 2, 50125 Firenze, Italy*
[2]*INAF - Osservatorio Astrofisico di Arcetri, Largo Enrico Fermi 5, 50125 Firenze, Italy*
[3]*INAF - Osseravtorio Astronomico di Roma, via di Frascati 33, 00040 Monteporzio Catone, Italy*
[4]*Kapteyn Astronomical Institute, Landlaven 12, 9747 AD Groningen, the Netherlands*

ABSTRACT

We present a semi-analytical model for the formation and evolution of a high-redshift quasar (QSO). We reconstruct a set of hierarchical merger histories of a 10^{13}-$M_\odot$ dark matter halo and model the evolution of the corresponding galaxy and of its central supermassive black hole. The code GAMETE/QSODUST consistently follows (i) the black hole assembly via both coalescence with other black holes and gas accretion; (ii) the build-up and star formation history of the quasar host galaxy, driven by binary mergers and mass accretion; (iii) the evolution of gas, stars and metals in the interstellar medium (ISM), accounting for mass exchanges with the external medium (infall and outflow processes); (iv) the dust formation in supernova (SN) ejecta and in the stellar atmosphere of asymptotic giant branch (AGB) stars, dust destruction by interstellar shocks and grain growth in molecular clouds; and (v) the active galactic nucleus feedback which powers a galactic-scale wind, self-regulating the black hole growth and eventually halting star formation.

We use this model to study the case of SDSS J1148+5251 observed at redshift 6.4. We explore different star formation histories for the QSO host galaxy and find that Population III stars give a negligible contribution to the final metal and dust masses due to rapid enrichment of the ISM to metallicities $>Z_{cr} = 10^{-6}$–$10^{-4}\,Z_\odot$ in progenitor galaxies at redshifts >10. If Population II/I stars form with a standard initial mass function (IMF) and with a characteristic stellar mass of $m_{ch} = 0.35\,M_\odot$, a final stellar mass of $(1$–$5) \times 10^{11}\,M_\odot$ is required to reproduce the observed dust mass and gas metallicity of SDSS J1148+5251. This is a factor of 3–10 higher than the stellar mass inferred from observations and would shift the QSO closer or on to the stellar bulge–black hole relation observed in the local Universe; alternatively, the observed chemical properties can be reconciled with the inferred stellar mass, assuming that Population II/I stars form according to a top-heavy IMF with $m_{ch} = 5\,M_\odot$. We find that SNe dominate the early dust enrichment and that, depending on the shape of the star formation history and on the stellar IMF, AGB stars contribute at $z < 8$–10. Yet, a dust mass of $(2$–$6) \times 10^8\,M_\odot$ estimated for SDSS J1148+5251 cannot be reproduced considering only stellar sources, and the final dust mass is dominated by grain growth in molecular clouds. This conclusion is independent of the stellar IMF and star formation history.

Key words: stars: AGB and post-AGB – supernovae: general – dust, extinction – galaxies: evolution – galaxies: high-redshift – quasars: general.

1 INTRODUCTION

The presence of large dust masses in high-redshift quasars (QSOs) has been revealed by millimetre and submillimetre observations of

samples of $5 < z < 6.4$ QSOs in the Sloan Digital Sky Survey (SDSS) (Bertoldi et al. 2003; Priddey et al. 2003; Robson et al. 2004; Beelen et al. 2006; Wang et al. 2008). The detection of the dust thermal emission and inferred far-infrared (FIR) luminosities of these objects suggests masses of warm ($T < 100$ K) dust of a few $10^8\,M_\odot$. Observations of QSOs and galaxies at high redshift are strongly affected by the presence of dust, and our ability

★E-mail: valiante@arcetri.astro.it

to interpret the observed properties of high-redshift sources depends on a detailed understanding of the star formation history (SFH) and the history of metal and dust pollution in their interstellar medium (ISM). Dust properties, such as grains' chemical composition and size distribution, are of primary importance in modelling the extinction curves in both the local Universe (Cardelli, Clayton & Mathis 1989; Pei 1992; Weingartner & Draine 2001) and at high redshifts (Maiolino et al. 2004; Stratta et al. 2007; Gallerani et al. 2010). Yet, the origin of dust at such early epochs is still unclear.

Among the stellar sources, the cool and dense atmosphere of asymptotic giant branch (AGB) stars and the expanding ejecta of core-collapse supernovae (SNe) offer the most viable sites of dust grain condensation. A SN origin has often been advocated as the only possible explanation for the large amount of dust observed in QSOs since it is usually assumed that low- and intermediate-mass stars ($m_* < 8\,M_\odot$) must evolve on a time-scale comparable to the age of the Universe at $z \geq 6$ (about 1 Gyr, Morgan & Edmunds 2003; Marchenko 2006; Dwek, Galliano & Jones 2007) before they reach the dust-producing stages. This scenario has been tested through observations of the reddened quasar SDSS J1048+46 at $z = 6.2$ (Maiolino et al. 2004) and of the spectral energy distribution of the $z = 6.29$ GRB 050904 (Stratta et al. 2007) and $z \sim 5$ GRB 071025 (Perley et al. 2010) sources. In these sources, the inferred dust extinction curve is different from any of the extinction curves observed at low z, and it shows a very good agreement with the extinction curve predicted for the dust formed in SN ejecta. This is an indication that the properties of dust may evolve beyond $z \geq 5$–6. In a recent study, Gallerani et al. (2010) find that the extinction curves of a sample of QSOs with $4 \leq z \leq 6.4$ deviate from the Small Magellanic Cloud (SMC) extinction curve (the one which better describes the $z < 2$ quasar reddening), suggesting that production mechanisms and/or dust processing into the ISM must be different at high redshift.

On the theoretical side, the evolution of dust in the early Universe is still poorly understood. Some of the models developed so far are still consistent with the scenario where most of the dust in QSOs at $z \sim 6$ is produced by SNe. However, these estimates either neglect dust destruction by interstellar shocks (Maiolino et al. 2006; Li et al. 2008) or make extreme assumptions on SN dust condensation factors (Dwek et al. 2007). In addition, it has been shown that only 2–20 per cent of the newly condensed dust survives the passage of the SN reverse shock, and grains are reduced both in number and in size, depending on the surrounding ISM density as well as on dust composition (see Bianchi & Schneider 2007; Nozawa et al. 2007; Bianchi, Schneider & Valiante 2009).

In a previous paper (Valiante et al. 2009, hereinafter V09), we showed that AGB stars can provide a non-negligible contribution to dust formation at high z, being able to produce dust already 30–40 Myr after the onset of SF, which is about the mean lifetime of a $\leq 8\,M_\odot$ star (see e.g. Padovani & Matteucci 1993; Raiteri, Villata & Navarro 1996). In particular, for a standard stellar initial mass function (IMF), the characteristic time-scale at which AGB stars dominate dust production ranges between 150 and 500 Myr, depending on the assumed SFH and on the stellar initial metallicity. Hence, we concluded that these stellar dust sources must be taken into account when modelling dust evolution at high redshift. In V09, we applied a simple chemical evolution model with dust to the host galaxy of the $z = 6.4$ SDSS J1148+5251 (hereinafter J1148) QSO, using as an input to the model the SFH obtained in a numerical simulation by Li et al. (2007); this simulation predicts that a large stellar bulge is already formed at $z = 6.4$, in agreement with

the local supermassive black hole (SMBH)–stellar mass relation, through a series of strong bursts triggered by galaxy mergers in the hierarchical evolution of the system. We found that the total mass of dust predicted at $z = 6.4$ is within the range of values inferred by observations of J1148, with a substantial contribution (80 per cent) of AGB dust. We concluded that stellar sources can account for the huge dust mass observed at these early cosmic epochs, even when the dust destruction by SN shocks is taken into account, at the price of having a total stellar mass of $\sim 10^{12}\,M_\odot$, which can hardly be reconciled with the dynamical mass of $\sim 5 \times 10^{10}\,M_\odot$ inferred from CO observations within 2.5 kpc from the QSO centre (Walter et al. 2004).

The above critical point has been recently emphasized by Michalowski et al. (2010) who showed that, using stellar masses approximated as the difference between the dynamical and H_2 gas masses for $5 < z < 6.5$ QSOs, stellar sources of dust are not efficient enough to account for the dust mass inferred in these systems. Therefore, they suggest additional non-stellar dust formation mechanisms, in particular, significant dust grain growth in the ISM of these QSOs. Indeed, dust grains formed in stellar outflows can serve as growth centres for the accretion of icy mantles in dense molecular clouds (MCs, see e.g. Draine 1990). It is already well known that MC-grown dust is the dominant component in the Milky Way (see e.g. Zhukovska, Gail & Trieloff 2008). Given the large masses of molecular gas detected in CO for most of these systems, Draine (2009) suggested that the bulk of their dust mass is the result of grain growth and that SNe are required to produce the metals that compose the grains and the 'seed' grain surface area on which more material can grow in MCs.

In this work, we investigate the nature of dust in high-z QSO host galaxies, focusing in particular on J1148 at $z = 6.4$. To this aim, we have improved the semi-analytic code GAMETE (GAlaxy MErger Tree and Evolution), developed by Salvadori, Schneider & Ferrara (2007, hereinafter SSF07), to model the hierarchical assembly and merger history of a QSO host galaxy at $z = 6.4$, together with its central SMBH, including the feedback from the active galactic nucleus (AGN) in the form of a galactic-scale wind. The chemical evolution network has also been modified to describe the evolution of dust, taking into account the specific stellar lifetimes, and the evolution of dust in the ISM through destruction by interstellar shocks and dust growth in MCs. This code, which we will refer to as GAMETE/QSODUST, will enable us to overcome the main limitations of V09 analysis, namely (i) we will be able to model different possible SFHs for J1148, discussing their impact on the chemical properties of the QSO host and, in particular, on the final dust mass; and (ii) we will be able to explore the relative importance of stellar sources of dust (SNe and AGB stars) and of grain growth in MCs. At the same time, the model can be constrained using the properties directly observed or inferred from observations of J1148, such as the mass of the central BH, the total mass of gas and stars, and the mass of metals and dust.

This paper is organized as follows. In Section 2, we will introduce the main physical properties of the QSO J1148 and its host galaxy, discussing the observational uncertainties. In Section 3, we will briefly summarize the basic features of the original GAMETE code and present the parameters adopted to simulate the hierarchical assembly of a QSO host halo at $z = 6.4$. In Section 4, we will discuss the new features of the code, which allow us to follow the formation and evolution of the central BH and its effects on the parent host galaxy through AGN-driven feedback. In Section 5, we describe the chemical evolution network, including the evolution of dust in the ISM. In Section 6, we will present the results and in

Section 7, we will discuss their implications. Finally, in Section 8, we will draw the main conclusions of this work.

In what follows, we adopt a Λ cold dark matter cosmology with $\Omega_m = 0.24$, $\Omega_\Lambda = 0.76$, $\Omega_b = 0.04$ and $H_0 = 73 \, \text{km s}^{-1} \, \text{Mpc}^{-1}$. The age of the Universe at $z = 6.4$ is 900 Myr.

2 J1148: A QSO AT REDSHIFT 6.4

In this section, we briefly summarize the physical properties of this extremely luminous QSO and of its host galaxy which have been derived observationally. The full list of properties, and observational uncertainties, is provided at the end of this section.

2.1 Dark matter host halo mass and AGN properties

The mass of the dark matter (DM) halo where J1148 is hosted, M_h, is usually estimated by requiring that the number density in haloes with masses $\geq M_h$ at $z \sim 6$ matches the observed space density of QSOs at the same redshift (Fan et al. 2004). Depending on the cosmological model, this generally yields $M_h = 10^{12}\text{–}10^{13} \, \text{M}_\odot$. The space density of observed QSOs with average redshift $\langle z \rangle = 6$ and luminosity $M_{1640} < -26.7$ is $(6.4 \pm 2.4) \times 10^{-10} \, \text{Mpc}^{-3}$ (Fan et al. 2004). For our adopted cosmological model, this would require a minimum halo mass of $\sim 3 \times 10^{12} \, \text{M}_\odot$. To compare with previous analyses (Volonteri & Rees 2006; V09), in this work, we generate Monte Carlo realizations of the merger histories adopting a value of $M_h = 10^{13} \, \text{M}_\odot$. The implications of a different halo mass and redshift will be addressed in a forthcoming paper, where a larger sample of QSOs will be investigated.

J1148 is a very luminous QSO with the absolute AB magnitude of the continuum in the rest frame at 1450 Å of $M_{1450} = -27.82$ mag (Fan et al. 2003). Assuming a power law $f_\nu \propto \nu^\alpha$ with $\alpha = -0.5$, the corresponding B-band magnitude[1] and luminosities are $M_B = -28.3$ and $L_B = 5.2 \times 10^{12} \, \text{L}_\odot$, where the effective wavelength of the B band is 4400 Å.

The energy requirement to power such luminosity suggests the presence of a BH mass of at least several billion solar masses. A virial estimate of the BH mass of $3 \times 10^9 \, \text{M}_\odot$ was obtained by Willott, McLure & Jarvis (2003) using the Mg II $\lambda 2800$ linewidth and the scaling relations derived by McLure & Jarvis (2002). Using the same scaling relations, but also the virial estimator provided by Vestergaard (2002), Barth et al. (2003) consistently found a BH mass in the range $(2\text{–}6) \times 10^9 \, \text{M}_\odot$ from the widths of both C IV $\lambda 1549$ and Mg II emission lines. Besides a factor of 2.5–3 estimated uncertainty in the adopted scaling relations, this method assumes that the dynamic of the line-emitting gas is dominated by gravitational forces. Note, however, that for objects radiating close to the Eddington limit, the effect of radiation pressure cannot be neglected and may lead to a non-negligible upward correction of the estimated BH masses (Marconi et al. 2008; Lamastra et al. 2010).

2.2 Host galaxy properties

High-resolution Very Large Array observations of J1148 have enabled to resolve CO(3–2) line emission both spatially and in

terms of velocity (Walter et al. 2004). The molecular gas is extended to a radius of ~ 2.5 kpc from the centre and a total mass of $M_{H_2} = 1.6 \times 10^{10} \, \text{M}_\odot$ has been derived, assuming a CO intensity-to-gas mass conversion factor appropriate for ultraluminous infrared galaxies (ULIRGs, Walter et al. 2004). Assuming that the gas is gravitationally bound and forms an inclined disc with inclination angle i, Walter et al. (2004) infer a dynamical mass of $M_{dyn} \sin^2 i \sim 4.5 \times 10^{10} \, \text{M}_\odot$. The molecular disc inclination angle is the main source of uncertainty in the dynamical mass estimates (Wang et al. 2010). Walter et al (2004) correct for an inclination of $65°$, on the basis of the broad CO full width at half-maximum detected, obtaining $M_{dyn} \sim 5.5 \times 10^{10} \, \text{M}_\odot$ with 50 per cent uncertainty.

The derivation of the stellar bulge mass is extremely uncertain. Indeed, this can be estimated either by extrapolating the local M_{BH}–M_* relation (Marconi & Hunt 2003; Haring & Rix 2004) at high redshift, $M_{BH}/0.0014 \sim 2.14 \times 10^{12} \, \text{M}_\odot$ (if a BH mass of $3 \times 10^9 \, \text{M}_\odot$ is considered), or by subtracting from the observed dynamical mass the H_2 gas mass, $M_* \sim M_{dyn} - M_{H_2} \sim 3.9 \times 10^{10} \, \text{M}_\odot$. It is evident that these estimates are inconsistent, since they differ by almost two orders of magnitude. Such a discrepancy persists, though alleviated, even if we assume that the stellar bulge mass of the host galaxy of J1148 was 10 times the scalelength of the molecular gas emission. Assuming a density profile of $\rho \propto r^{-2}$, the stellar mass would be $M_* \sim 3.9 \times 10^{11} \, \text{M}_\odot$ (Walter et al. 2004).

Further constraints on the evolution of the QSO host galaxy come from observations of the gas-phase metallicity and elemental abundances in both the broad- and the narrow-line regions (BLRs and NLRs, respectively). BLRs' metallicity tracers are emission-line ratios, such as FeII/Mg II (e.g. Barth et al. 2003), N v/C IV (e.g. Pentericci et al. 2002) and (Si IV+O IV)/C IV (Nagao, Marconi & Maiolino 2006; Juarez et al. 2009), together with other metal lines like C II (e.g. Maiolino et al. 2005) and O I (Becker et al. 2006). The observed ratios are similar to those observed in low-z QSOs, indicating BLRs' metallicities which are several times solar, $\sim 7 \, Z_\odot$ (Nagao et al. 2006 Juarez et al. 2009) and suggesting that the ISM of the QSO host was significantly enriched by heavy elements. However, the BLRs are small nuclear regions, of less than a few pc, containing a total mass of $\sim 10^4 \, \text{M}_\odot$; thus, we consider such a high metallicity as an upper limit. Conversely, NLRs have larger masses and a size which is roughly comparable to the size of the host galaxy and represent a good tracer of the chemical properties on galactic scales, since their metal content reflects the past SFH of the galaxy (Matsuoka et al. 2009, and references therein). To date, however, measurements of the NLRs' metallicity only up to redshift 4 are available. Focusing on the C IV/He II and C III/C IV flux ratios, Matsuoka et al. (2009) point out that even NLRs show no significant metallicity evolution with redshift, up to $z \sim 4$. For the highest redshift sample, these authors find a NLR metallicity of about $1.32^{+1.57}_{-1.10} \, Z_\odot$. We adopt this value as a lower limit for the ISM metallicity of J1148.

2.3 Dust mass, FIR luminosity and SFR

The dust present in the host galaxy is probably characterized by multitemperature components: hot (~ 100 K), warm (30–80 K) and cold (10–20 K). The hot dust component, directly heated by the AGN activity, has been observed for several $z \sim 6$ QSOs with *Spitzer* (Charmandaris et al. 2004; Jiang et al. 2010) and represents the least contribution to the total mass of dust. Warm dust, associated to starburst regions, dominates the emission in the rest-frame FIR. For J1148, it has been observed in four bands: at 1.2 mm (Bertoldi et al. 2003), 850 μm, 450 μm (Robson et al. 2004), and 350 μm

---

[1] Schmidt, Schneider & Gunn (1995) find $M_B = M_{1450} + 2.5\alpha \log (4400 \, \text{Å}/1450 \, \text{Å}) + 0.12$, where the factor 0.12 comes from the zero-point difference between the AB and the Vega-based magnitude systems for QSO-like spectra.

Table 1. Dust temperature, dust mass and FIR luminosity resulting from the χ^2 fit of the four observed photometric points of J1148 (see text). Each line refers to the value inferred from the fit taking the dust absorption coefficient as specified by the corresponding κ_0 and β. These values have been chosen following quoted values in the literature and assuming specific dust grain models.

Reference	κ_0 (cm^2 g^{-1})	λ_0 (µm)	β	T_d (K)	M_{dust} (M$_\odot$)	L_{FIR} (L$_\odot$)
a	7.5	230	1.5	58	3.16×10^8	2.32×10^{13}
b	30	125	2.0	49	2.91×10^8	2.09×10^{13}
c	0.4	1200	1.6	56	4.29×10^8	2.27×10^{13}
d	34.7	100	2.2	47	4.78×10^8	2.02×10^{13}
e	40	100	1.4	60	1.86×10^8	2.38×10^{13}

References: a = Bertoldi et al. (2003); b = Robson et al. (2004); c = Beelen et al. (2006); d = fit to the Weingartner & Draine (2001) model for the SMC in the spectral range 40–200 µm; and e = SN dust model by Bianchi & Schneider (2007).

(Beelen et al. 2006). The cold dust, finally, may represent the largest component. Its emission, however, would be hidden by the warmer component even if its mass were 1.5–3 times larger (Dunne et al. 2000).

In the rest-frame FIR, the emission is optically thin, $\tau_d(\lambda) \ll 1$, and the dust mass can be estimated from the flux observed in a given band S_{ν_0} as

$$M_{dust} = \frac{S_{\nu_0} d_L^2(z)}{(1+z) \kappa_d(\nu) B(\nu, T_d)}, \tag{1}$$

where $\kappa_d(\nu)$ is the opacity coefficient per unit dust mass, $B(\nu, T_d)$ is the Planck function for a dust temperature T_d and d_L is the luminosity distance to the source. In the Rayleigh–Jeans part of the spectrum, dust radiates as a 'grey body' with $\kappa_d(\nu) = \kappa_0(\nu/\nu_0)^\beta$. Integrating over the spectrum, one obtains the corresponding FIR luminosity,

$$L_{FIR} = 4\pi M_{dust} \int \kappa_d(\nu) B(\nu, T_d) d\nu.$$

Although, in principle, with four photometric points, it could be possible to simultaneously fit M_{dust}, β and T_d, at the redshift of J1148, the observations do not fully sample the Rayleigh–Jeans part of the spectrum, preventing the determination of β. Therefore, the estimated mass of dust and FIR luminosities for J1148 quoted in the literature have been derived under different assumptions for β and κ_0. The resulting dust masses, FIR luminosities and dust temperatures are listed in Table 1 and have been calculated through a χ^2 fit using all the observed points in the range 350 µm–1200 mm. Taking into account the intrinsic error on the estimated fluxes, the typical error associated to a single fit is 25 per cent. As it can be inferred from the table, we have considered, in addition to dust absorption coefficients already adopted in previous works (cases a–c), a fit to the Weingartner & Draine (2001) model for the SMC in the relevant frequency range (case d) as well as the dust optical properties expected for SN dust following the model by Bianchi & Schneider (2007, case e).

The resulting dust masses and temperatures are very sensitive to the adopted dust absorption coefficient and spectral index with values in the range $(1.86–4.78) \times 10^8$ M$_\odot$. In what follows, we will assume an average dust mass of 3.4×10^8 M$_\odot$ with error bars computed assuming the minimum and maximum values quoted in the table. It is important to note that a mixture of SMC and SN extinction curves (30 per cent SMC and 70 per cent SN) is found to best fit the extinction properties of a sample of QSOs with $3.9 \leq z \leq 6.4$, including J1148 (Gallerani et al. 2010).

From Table 1, we also infer an average FIR luminosity of $L_{FIR} = 2.2 \times 10^{13}$ L$_\odot$ with 15 per cent uncertainty associated to the fit. Assuming that the dominant dust-heating mechanism is radiation from young stars, it is possible to estimate the star formation rate (SFR) using the relationship between FIR luminosity and SFR derived by Kennicutt (1998),[2]

$$\frac{SFR}{1 M_\odot yr^{-1}} = \frac{L_{FIR}}{5.8 \times 10^9 L_\odot},$$

which implies a SFR $\sim (3.8 \pm 0.57) \times 10^3$ M$_\odot$ yr^{-1} (Bertoldi et al. 2003). Such a high SFR is also supported by the first detection of the carbon [C II] line at 158 µm (Maiolino et al. 2005), where a SFR $\sim 3 \times 10^3$ M$_\odot$ yr^{-1} is estimated combining the above conversion with the [C II] line-to-FIR luminosity ratio obtained from photodissociation region models.

It is clear that if the AGN contributes to dust heating, the corresponding SFR would be much lower, consistent with the value that would be inferred from the observed gas mass by a simple application of the Schmidt–Kennicutt law. In fact, using the relation proposed by Daddi et al. (2010) to fit local ULIRGs and submillimetre galaxies and QSOs,

$$\log \Sigma_{SFR}/(M_\odot \ yr^{-1} \ kpc^{-2}) = 1.42 \times \log \Sigma_{gas}/(M_\odot \ pc^{-2}) - 2.93,$$

and assuming that the SFR is confined to the same central 2.5 kpc where molecular gas emission has been detected, we find a SFR ~ 180 M$_\odot$ yr^{-1} consistent with previous findings by Dwek et al. (2007) and Li et al. (2007).

Summarizing, the observed/inferred properties of J1148 used as reference values in this work are as follows:

(i) A DM halo mass of $M_h = 10^{13}$ M$_\odot$, which is assumed to host the $z = 6.4$ QSO J1148.

(ii) A SMBH mass of $M_{BH} \sim 3^{+3.0}_{-1.0} \times 10^9$ M$_\odot$ inferred from the Mg II λ2800 and C$_{IV}$ λ1549 linewidths (Barth et al. 2003; Willott et al. 2003).

(iii) A dynamical and molecular gas mass of $M_{dyn} = (5.5 \pm 2.75) \times 10^{10}$ M$_\odot$ and $M_{H_2} = 1.6 \times 10^{10}$ M$_\odot$, derived from observations of the CO(3–2) line emission and assuming an inclination angle $i = 65°$ (Walter et al. 2003).

(iv) A final stellar mass ranging from $M_* = (3.9 \pm 2.75) \times 10^{10}$ M$_\odot$ (computed as the difference between the dynamical and

_____

[2] The conversion factor 5.8×10^9 has been derived assuming a mean luminosity for a 10–100 Myr burst, stars with solar abundances and a Salpeter IMF (see the original Kennicutt 1998 paper for details).

molecular gas masses given above) up to $M_* \sim 10^{12} \, \mathrm{M_\odot}$, which is the one inferred if the local M_{BH}–M_* relation were to hold even at redhift 6.4.

(v) An ISM metallicity of $Z = 1.32^{1.57}_{1.10} \, Z_\odot$, estimated from observations of NLRs in QSOs (Matsuoka et al. 2009). We refer to this value as a lower limit for the metallicity of J1148.

(vi) A total mass of dust of $M_{dust} = 3.4^{+1.38}_{-1.54} \times 10^8 \, \mathrm{M_\odot}$, computed using equation (1) and the parameters given in Table 1.

(vii) An upper limit to the SFR, $\sim(3.8 \pm 0.57) \times 10^3 \, \mathrm{M_\odot \, yr^{-1}}$, obtained assuming that dust heating is entirely due to the radiation from young stars.

3 MODEL DESCRIPTION

Here we describe our Monte Carlo semi-analytical model, GA-METE/QSODUST, which follows the formation and evolution of the quasar SMBH and its host galaxy in the hierarchical scenario of structure formation. In this framework, a galaxy forms through a series of merging episodes of lower mass fragments, called *progenitors*. The code is divided into two main blocks: the first block runs backwards in time and it is needed to reconstruct the merger tree history of the assumed 10^{13}-$\mathrm{M_\odot}$ DM halo at $z = 6.4$ (see Section 2); the second block runs forwards in time and allows us to follow the evolution of the baryonic component and the growth of the nuclear BH. In this way, it is possible to simulate several hierarchical merger histories of the host DM halo and then follow the build up of the quasar and the evolution of the host galaxy properties along these various formation paths. Each formation path will result in a peculiar redshift evolution for the host galaxy properties. However, in order to draw some general conclusions, in what follows, we will show the results obtained by averaging over all the simulated hierarchical merger histories.

In the following sections, we will briefly describe the Monte Carlo algorithm used to reconstruct the hierarchical merger tree of the 10^{13}-$\mathrm{M_\odot}$ DM halo hosting the QSO at $z = 6.4$ (see SSF07 for a detailed description of the algorithm) and the semi-analytical model which follows the evolution of gas, stars and metals along the hierarchical build-up of the galaxy (see Salvadori, Ferrara & Schneider 2008, hereinafter SFS08, for more details). Then, we will introduce in details the new features of the GAMETE/QSODUST version implemented to follow the evolution of the central SMBH and of the dust mass.

3.1 The hierarchical merger history

The possible hierarchical merger histories of an $M_h = 10^{13} \, \mathrm{M_\odot}$ DM halo at $z = 6.4$ are reconstructed using a *binary* Monte Carlo algorithm with *mass accretion* (e.g. Cole et al. 2000; Volonteri, Haardt & Madau 2003), based on the Extended Press–Schechter (EPS) theory (e.g. Lacey & Cole 1993).

At each increasing redshift, a DM halo can either lose part of its mass or lose mass and fragment into two progenitors with random masses in the range $M_{res} < M < M_h/2$, where M_{res} is a threshold mass representing the model resolution limit: haloes with $M < M_{res}$ are not considered as progenitors, but account for the surrounding medium in which other haloes are embedded and from which they accrete mass and virialize.

The resolution mass, M_{res}, along with the redshift interval chosen to sample the merger history, represents the free parameters of the model and is constrained in order to (i) prevent multiple fragmentations; (ii) resolve all the progenitors with masses above a given physical threshold; (iii) reproduce the EPS predictions; and
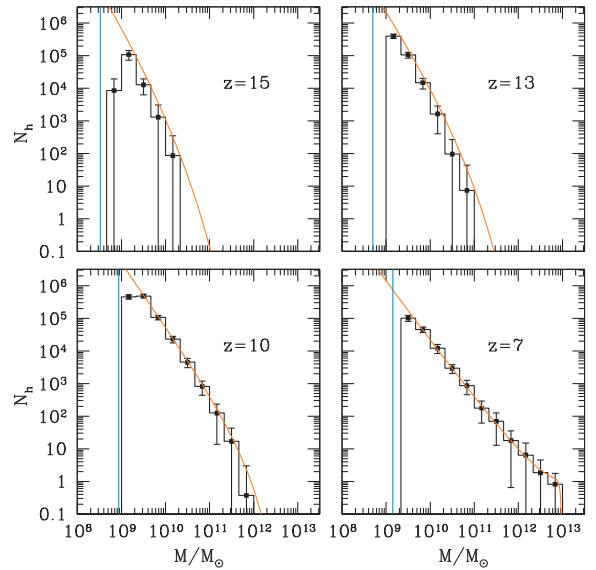

Figure 1. Number of progenitors of a QSO host halo of mass $10^{13} \, \mathrm{M_\odot}$ at $z = 6.4$ as a function of mass at four different redshifts: $z = 15, 13, 10$ and 7 (from the top left-hand to bottom right-hand panel). In each panel, the histograms represent averages over 50 realizations of the merger tree and the error bars indicate the Poissonian error on the counts in each mass bin; the solid lines show the predictions of EPS theory and the vertical lines indicate the values of the resolution mass at the corresponding redshift.

(iv) control the computational cost. Given the above requirements, we assume that $M_{res}(z) = 10M(T_{vir} = 10^4 \, \mathrm{K}, z)$, where $M(T_{vir} = 10^4 \, \mathrm{K}, z)$ is the mass of a DM halo with a virial equilibrium temperature of $10^4 \, \mathrm{K}$ at redshift z. The merger tree is computed using 5000 redshift intervals logaritmically spaced in the expansion factor between $z = 6.4$ and 37. In Fig. 1, we compare the mass function of the progenitor haloes averaged over 50 possible hierarchical merger histories with the EPS predictions. We can see that the agreement is extremely good at all redshifts ($z = 15, 13, 10, 7$).

We then use the produced merger trees as an input to reconstruct the formation and evolution of the quasar J1148 and its host galaxy through cosmic time.

3.2 Evolution along a merger tree

In what follows, we present a brief summary of the basic prescriptions proposed by SFS08 which are unchanged in the present version of the code. Note that in order to significantly reduce the high computational cost caused by the high number of redshift intervals, we are now considering as *star-forming* objects all DM haloes with masses equal to or greater than $M_{sf}(z) = 10M_{res}(z)$ (see Fig. 2).

In any star-forming halo, the SFR is taken to be proportional to the mass of cold gas,

$$\mathrm{SFR} = f_*(z)M_{gas}, \tag{2}$$

whose gradual accretion is regulated by an infall rate, dM_{inf}/dt (see SFS08 for the complete expression). The parameter $f_*(z)$ is the redshift-dependent global efficiency of SF per unit time. We will discuss this efficiency in detail in the next section.

In this model, Population III (Pop III) stars with an average mass of $200 \, \mathrm{M_\odot}$ are assumed to form if the gas metallicity is lower than a critical value $Z_{cr} = 10^{-4} \, Z_\odot$. Otherwise, if the gas metallicity exceeds the critical limit, low-mass (Pop II/I) stars are assumed to form according to a Larson IMF, which follows a Salpeter-like
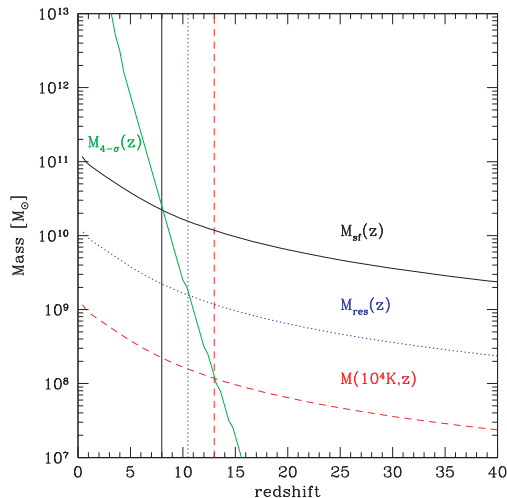
Figure 2. The threshold masses adopted in the code as a function of redshift. $M(10^4 \, \text{K}, z)$ is the mass of a halo with a virial temperature $T_{\text{vir}} = 10^4 \, \text{K}$, $M_{\text{res}}(z) = 10M(T_{\text{vir}}, z)$ is the minimum halo mass in the merger tree simulations and $M_{\text{sf}}(z)$ is the minimum halo mass to form stars, assumed to be equal to $100M(10^4 \, \text{K}, z)$. These masses are compared with the 4σ mass density fluctuation $M_{4\sigma}(z)$ (green solid line). When newly virialized haloes, in the merger tree, are less massive than $M_{4\sigma}(z)$, they do not host a seed BH. The redshift at which haloes are no more populated with seed BHs depends on the assumed threshold as indicated by the vertical lines. For the adopted minimum halo mass to form stars, $M_{\text{sf}}(z)$, we populate haloes down to redshift of about 8.

power law at the upper end but flattens below a characteristic stellar mass:

$$\phi(m) \propto m^{-(\alpha+1)} e^{-m_{\text{ch}}/m}, \qquad (3)$$

where $\alpha = 1.35$, $m_{\text{ch}} = 0.35 \, \text{M}_\odot$ and we normalize the integral of $m\phi(m)$ in the mass range 0.1–$100 \, \text{M}_\odot$ to unity. The evolution of very massive stars is rapid (they reach the end of their main-sequence phase in 3–5 Myr) and ends in a violent explosion as pair instability SNe (PISNe) which leave no remnants behind and significantly contribute to the metal enrichment of the ISM at the lowest metallicities. Thus, we can assume that Pop III stars die instantaneously, while less massive stars are assumed to evolve according to their appropriate stellar lifetime. In this work, the lifetimes of stars of different mass and metallicity are computed according to the parametric form proposed by Raiteri et al. (1996). As we will show in Section 6.3.2, our results are not sensitive to the adopted values for the mass of Pop III stars and of the critical metallicity.

Finally, the galactic outflows driven by SN explosions, $dM_{\text{ej,SN}}/dt$, are assumed to be proportional to the SN explosion rate (R_{SN}) divided by the escape velocity (v_{e}) squared:

$$\frac{dm_{\text{ej,SN}}}{dt} = \frac{2\epsilon_{\text{w}} E_{\text{SN}} R_{\text{SN}}}{v_{\text{e}}^2}, \qquad (4)$$

where ϵ_{w} is the SN-wind efficiency and E_{SN} is the average SN explosion energy (see SFS08 for further details).

3.3 New features

The new features implemented for the purposes of this work are (i) the growth of the BH (via both gas accretion and mergers with companion BHs); (ii) the effect of the AGN feedback on the host galaxy; (iii) the merger-driven starbursts, that is, bursts of SF episodes en-

hanced by haloes' binary merging; and (iv) the dust formation and evolution into the ISM. We will describe them in turn.

3.3.1 BH growth

It is usually assumed that SMBHs are assembled by mergers with other BHs and/or by accretion of the gas from the surrounding medium. Thus, the growth of a BH is determined by the seed BH properties (e.g. mass, redshift distribution and abundance), the efficiency of the accretion rate, the number of BH mergers and the dynamics of the coalesced BHs. Theoretical studies suggest that a seed BH with the mass in the range 10^2–$10^6 \, \text{M}_\odot$ can form either by the rapid collapse of Pop III stars (Heger & Woosley 2002) or by the direct collapse of massive hot ($T > 10^4 \, \text{K}$) and dense gas clouds induced by gravitational instabilities (e.g. Bromm & Loeb 2003; Begelman, Volonteri & Rees 2006; Volonteri & Natarajan 2009).

In this work, we assign a BH seed, $M_{\text{seed}} = 10^4 \, h^{-1} \, \text{M}_\odot$, to all the progenitor haloes corresponding to density fluctuations higher than 4σ ($M > M_{4\sigma}$) that exceed the threshold mass required to form stars ($M > M_{\text{sf}}$) for the first time in the merger tree. The evolution of these critical masses as a function of redshift is shown in Fig. 2. From this plot, we can infer that the probability, P, that a halo with $M > M_{\text{sf}}$ will host a seed BH depends on the redshift, other than on the specific formation history, and that $P \rightarrow 0$ for $z < 8$. Note that even assuming $P = 1$ for all the star-forming progenitors, the mass density parameter in seed BHs at $z = 6.4$ would be $\Omega_\bullet \sim 10^{-11}$, several orders of magnitude less than the SMBH density parameter estimated from nuclear BHs of nearby galaxies, $\Omega_{\text{SMBH}} (z = 0) = 2.9 \times 10^{-6}$ (Merloni & Heinz 2008). Indeed, seed BHs grow via binary mergers and gas accretion. The choice of the BH seed will be discussed in Section 6.1.

Following Tanaka & Haiman (2009), we assume that if the progenitor halo mass ratio, $\mu = M_{\text{s}}/M_{\text{p}}$ (where M_{s} is the mass of the secondary smaller halo and M_{p} is the mass of the primary larger halo), is >1/20, the BHs coalesce efficiently over the same time-scale as that of their host haloes, adding their masses linearly.[3] Conversely, if the mass ratio of the two progenitors is smaller than 1:20, only the largest of two original BHs survives as a nuclear BH, the less massive one is assumed to end up as a satellite and its evolution along the merger tree is no longer followed.

It is known that the BH produced by a coalescence receives a gravitational recoil (kick velocities $\geq 100 \, \text{km} \, \text{s}^{-1}$) due to the net linear momentum accumulated by the asymmetric gravitational wave emission (Baker et al. 2006; Campanelli et al. 2006). As a consequence of this effect, the recoiling BH could be kicked out of its host halo or displaced in underdense regions, thus reducing the gas accretion rate. Tanaka & Haiman (2009) have added in their Monte Carlo code an explicit calculation of the orbits of kicked BHs and self-consistently included their corresponding time-dependent accretion rate. We do not attempt to do a similar analysis here and we neglect this effect; note, however, that in our model we expect the number of BHs ejected out of their host halo to be modest since the escape velocities of haloes with masses $\geq M_{\text{sf}}(z)$ are $\geq 110 \, \text{km} \, \text{s}^{-1}$.

In GAMETE/QSODUST, BHs are allowed to grow in mass by accreting gas from the surrounding medium. This process is triggered by gas-rich halo mergers and is regulated both by SF, which consumes gas by converting it into stars, and by AGN feedback,

---

[3] This condition is derived requiring that the halo-merger time-scale is shorter than the Hubble time (see Tanaka & Haiman 2009 for more details).

which reduces the amount of material available for accretion. In our formulation, the central BH accretes gas at a rate given by $\dot{M}_{accr} = \min(\dot{M}_{Edd}, \dot{M}_{BHL})$, where $\dot{M}_{Edd}$ is the Eddington rate,

$$\dot{M}_{Edd} = \frac{4\pi G M_{BH} m_p}{\epsilon_r \sigma_T c}, \tag{5}$$

and $\dot{M}_{BHL}$ is the Bondi–Hoyle–Lyttleton (BHL) accretion rate,

$$\dot{M}_{BHL} = \frac{4\pi \alpha G^2 M_{BH}^2 \rho_{gas}(r_A)}{c_s^2}. \tag{6}$$

In the above equations, G is the gravitational constant, m_p is the proton mass, σ_T is the Thomson cross-section, c is the light speed, c_s is the sound speed, $\rho_{gas}(r_A)$ is the gas density evaluated at the radius of gravitational influence of the BH (or Bondi accretion radius), $r_A = 2GM_{BH}/c_s^2$ and α is a dimensionless parameter (see below); in equation (5), the parameter ϵ_r is the radiative efficiency, which determines the conversion efficiency of mass accretion into energy released as radiated luminosity, and it is fixed to 0.1 (Shakura & Sunyaev, 1973).

We adopt a gas density distribution described by a singular isothermal sphere profile with a flat core:

$$\rho(R) = \frac{\rho_{norm}}{1 + (R/R_{core})^2}, \tag{7}$$

where $R_{core} = 0.012 R_{vir}$ is the size of the flat core, R_{vir} is the virial radius and ρ_{norm} is the normalization constant; the profile is normalized such that, at each time-step, the total gas mass, M_{gas}, is enclosed within the virial radius. The factor α which appears in equation (6) does not appear in the original analysis of Bondi & Hoyle (1944) and Hoyle & Lyttleton (1939), but has been introduced by Springel, Di Matteo & Hernquist (2005) as a numerical correction factor, to compensate for the limitations of the numerical simulations. In fact, present simulations lack both the resolution and the physics to model the multiphase ISM, and tend to strongly underestimate the Bondi–Hoyle accretion rate; values of $100 \leq \alpha \leq 300$ are commonly adopted in the literature (Di Matteo, Springel & Hernquist 2005; Springel et al. 2005; Sijacki et al. 2007; Di Matteo et al. 2008; see, however, Booth & Schaye 2009 who parametrize α as a function of density). As it will be discussed in the following sections, we also assume a constant α and fix its value in order to reproduce the observed BH mass of J1148.

3.3.2 AGN feedback

It is natural to expect that a quasar shining at, or close to, its limiting Eddington luminosity can generate a powerful galactic wind and eventually terminate the accretion process that feeds it. If the energy in the outflow liberates as much energy as the binding energy of the gas in a dynamical time, the feedback from the accreting BH can be self-regulated (Silk & Rees 1998; Wyithe & Loeb 2003). Hydrodynamical simulations suggest that a BH accreting at high rates releases enough energy to drive galactic-scale outflows of gas (Di Matteo et al. 2005; Springel et al. 2005; Ciotti, Ostriker & Proga 2009, 2010). The mechanism by which the energy released by the accreting BH is coupled to the surrounding medium is currently under debate (see Ciotti et al. 2010, and references therein). The energy transfer rate is commonly parametrized as (e.g. Springel et al. 2005)

$$\dot{E}_{fbk} = \epsilon_{w,AGN} \epsilon_r \dot{M}_{accr} c^2, \tag{8}$$

where the parameter $\epsilon_{w,AGN}$ is the coupling efficiency and it is usually assumed to be a free parameter of the simulation, independent of the environment and gas properties.

Note that recently Sijacki et al. (2007) have differentiated between a 'quasar-mode' and a 'radio-mode' feedback, depending on the accretion rate. In particular, BH-powered winds are related to the luminous quasar activity and are efficient for high accretion rates. They are expected to be more powerful than starburst-driven winds and should be able to sweep away a significant amount of gas from the deep potential well of their massive host galaxies. Once the obscuring material is swept away from the centre of the system, the quasar enters its visible phase in which it outshines the entire galaxy (quasar mode). In the low-accretion-rate regime, which is subdominant in terms of BH mass growth, the feedback is characterized by AGN-driven bubbles; this regime can be identified with radio galaxies in clusters (radio mode). The BH accretion rate which signs the transition between these two modes is usually assumed to be $\dot{m}_{crit} = (\dot{M}_{accr}/\dot{M}_{Edd}) = 10^{-2}$ (Sijacki et al. 2007); thus, since here we are not interested in the radio-mode regime, we only activate the BH feedback when the accretion rate is supercritical.

When the above condition is verified, we estimate the amount of the gas mass ejected out of the host halo per unit time as

$$\frac{dM_{ej,AGN}}{dt} = 2\epsilon_{w,AGN} \epsilon_r \left(\frac{c}{v_e}\right)^2 \dot{M}_{accr}, \tag{9}$$

where $M_{ej,AGN}$ is the mass of ejected gas and $v_e = (\frac{GM}{R_{vir}})^{1/2}$ is the escape velocity of the galaxy.

3.3.3 Bursting star formation mode

The SFH of the QSO host at $z = 6.4$ is the result of the SFHs of all its progenitor haloes. There are observational and theoretical indications that support the idea that galaxy mergers have a dramatic effect on their morphological evolution and SFH (see e.g. Mihos & Hernquist 1996; Woods & Geller 2007; Ellison et al. 2010; Cox et al. 2008, and references therein). In particular, enhanced central SF in interacting galaxies results from gaseous inflows that occur when the gas loses angular momentum through gravitational tidal torques produced primarily by the non-axisymmetric structure induced by the companion galaxies. Indeed, there is mounting evidence that near-equal-mass mergers (with mass ratios greater that 1:3) trigger the most vigorous star-forming galaxies in the local universe, the ULIRGs (see e.g. Genzel et al. 2001; Tacconi et al. 2002; Dasyra et al. 2006). Similarly, there is growing observational evidence for interaction-driven nuclear activity (see the recent review by Shankar 2009).

Based on a set of numerical simulations, Cox et al. (2008) have studied the effects of the galaxy mass ratio on merger-driven starbursts. They find that while mergers between nearly-equal-mass galaxies produce the most intense bursts of SF (major mergers), minor mergers produce relatively little enhancement with respect to the quiescent mode of SF. These simulations have been calibrated to reproduce the observed properties of local disc galaxies and may not be immediately extended to higher redshifts. The resulting fitting formulae have been implemented in semi-analytic models of galaxy evolution, which successfully reproduce a number of observations at $z \sim 0$ (Somerville et al. 2008).

Here we are interested in exploring the effects of different SFHs on the chemical properties of QSOs' host galaxies. Therefore, we investigate both quiescent and bursting models: in the first class of models, SF occurs only in a quiescent mode which is independent of the galaxy mergers' mass ratio; conversely, in the second class of models, an additional contribution to the stellar mass comes from galaxy major mergers. In order to explore a wide parameter space,

we parametrize the global redshift-dependent efficiency of SF per unit time that appears in equation (2) as

$$f_*(z) = (\epsilon_{\rm quies} + \epsilon_{\rm burst})/t_{\rm dyn}(z), \tag{10}$$

where $t_{\rm dyn}(z) = R_{\rm vir}/v_{\rm e}$ is the dynamical time, $\epsilon_{\rm quies}$ is the constant SF efficiency during the quiescent phase of the evolution and $\epsilon_{\rm burst}$ is the starburst efficiency expressed as a normalized Gaussian distribution of the mass ratio,

$$\epsilon_{\rm burst} = \frac{1}{\sqrt{2\pi}\sigma_{\rm burst}} {\rm e}^{-(\mu-\mu_{\rm crit})^2/2\sigma_{\rm burst}^2}. \tag{11}$$

The starburst efficiency peaks at the critical mass ratio $\mu_{\rm crit} = 1$ and the dispersion parameter controls the intensity of the burst for a given mass ratio. It is important to stress that since the merger rate and the mass ratio of merging haloes depend on the hierarchical merger history, variations in the parameter $\sigma_{\rm burst}$ allow to explore a wide range of SFHs, with lower values of $\sigma_{\rm burst}$ corresponding to fewer intense bursts over the history of the galaxy; as $\sigma_{\rm burst}$ decreases, the SFHs will be characterized by more frequent and less intense bursts, progressively approaching the quiescent SF mode. For our test cases, $\sigma_{\rm burst} = 0.05$, 0.1 and 0.25 corresponding to the maximum merger efficiencies (if $\mu = \mu_{\rm crit}$) of $\epsilon_{\rm burst} \simeq 8$, 4 and 1.6, respectively.

3.3.4 The evolution of dust

We compute the evolution of dust under the following assumptions: (i) both SNe and AGB stars contribute to dust production on different time-scales according to their stellar progenitors' lifetimes; (ii) there is no dust infall or outflow to/from the ISM, that is, the infalling gas is dust-free: only dust grain metals that are returned to the gas-phase ISM through destruction by interstellar shocks (i.e. dust that has been shocked by SNe) can be ejected out of the galaxy; (iii) a fraction $f_{\rm mc}$ of the dust mass is enclosed in dense MCs, $M_{\rm d}^{\rm mc}(t) = f_{\rm mc}M_{\rm d}(t)$; this component can grow through mass accretion of metals on to pre-existing grains in a time-scale $\tau_{\rm acc}$; and (iv) the remaining dust component, $M_{\rm d}^{\rm diff}(t) = (1 - f_{\rm mc})M_{\rm d}(t)$, is diffused in the ISM and can be destroyed by interstellar shocks in a time-scale $\tau_{\rm d}$.

The destruction and accretion time-scales depend on the properties of the ISM and on the cycling times between the cloud (cold and dense) and intercloud (warm/hot and diffuse) phases (e.g. Tielens et al. 1998, 2005). Thus, a multiphase description of the ISM would be required to properly follow the evolution of the two dust components, $M_{\rm d}^{\rm mc}$ and $M_{\rm d}^{\rm diff}$. Here, we make the simplifying assumption that a fixed fraction $f_{\rm mc} \sim 1/2$ (see e.g. Dwek 1998) of the total dust particles are located in MCs and thus can serve as growth centres for the accretion of icy mantles (e.g. Draine 1990).

Following Hirashita (1999), we model the dust accretion time-scale $\tau_{\rm acc}$ as

$$\tau_{\rm acc} = \frac{\tau_{\rm mc}}{X_{\rm cold}[1 - f_{\rm dep}(t)]}, \tag{12}$$

where $\tau_{\rm mc} = 3 \times 10^7$ yr is the typical lifetime of a MC (e.g. Tielens 1998) and $X_{\rm cold}$ is the fraction of cold gas in the ISM, which is set to unity in our one-phase scenario. Finally, $f_{\rm dep}(t)$ is the depletion factor, that is, the ratio between the mass of dust and the total mass in metals, $M_{\rm d}(t)/M_Z(t)$, which is computed at each time in each halo of the simulation. Only metals which are not already condensed into dust grains (i.e. gas-phase metals) are available for accretion. Typical values of this time-scale are in the range 10^7–10^8 yr (see Fig. 9 shown later).

The destruction time-scale, $\tau_{\rm d}$, that is, the lifetime of dust grains against destruction by thermal sputtering in high-velocity ($v > 150\,{\rm km\,s^{-1}}$) SN shocks is given by (e.g. Dwek & Scalo 1980; McKee 1989)

$$\tau_{\rm d} = \frac{M_{\rm ISM}(t)}{\epsilon_{\rm d}M_{\rm swept}R'_{\rm SN}}, \tag{13}$$

where $\epsilon_{\rm d}$ is the dust-destruction efficiency, $M_{\rm swept}$ is the effective ISM mass that is completely cleared of dust by a single SN remnant and $R'_{\rm SN} = f_{\rm SN}R_{\rm SN}$ is the effective SN rate for grain destruction, which takes into account that not all the SNe which interact with the ISM are efficient in destroying dust[4] (see e.g. McKee 1989; Tielens 2005); for PISNe, $f_{\rm SN} = 1$, and for core-collapse SNe, $f_{\rm SN} \sim 0.15$ (i.e. 15 per cent of all SNe in a stellar generation are efficient). Following McKee (1989), we compute the mass of the interstellar matter shocked to a velocity $v_{\rm sh}$ in the Sedov–Taylor stage, in a homogeneous ISM, as

$$M_{\rm swept} = 6800\,{\rm M_\odot}\frac{(E_{\rm SN}/10^{51}{\rm erg})}{(v_{\rm sh}/100\,{\rm km\,s^{-1}})^2}, \tag{14}$$

where $v_{\rm sh} \sim 200\,{\rm km\,s^{-1}}$ is the (minimum) non-radiative shock velocity and $E_{\rm SN}$ is the average SN explosion energy, assumed to be 2.7×10^{52} erg for PISNe and 1.2×10^{51} erg for core-collapse SNe. We adopt the dust-destruction efficiencies from Nozawa et al. (2006) for PISNe and from Jones, Tielens & Hollenbach (1996) for SNe. Assuming a reference value for the ISM density of $n_{\rm ISM} = 1\,{\rm cm^{-3}}$, we get $\epsilon_{\rm d} \sim 0.6(0.48)$ for PISNe (SNe). With these parameters, we find that for conditions which apply to the Milky Way galaxy ($M_{\rm ISM} \sim 5 \times 10^9\,{\rm M_\odot}$, $R'_{\rm SN} \sim 7.5 \times 10^{-3}\,{\rm yr^{-1}}$, McKee 1989), typical grain lifetimes are ~ 0.6 Gyr, in agreement with Jones et al. (1996).

4 THE CHEMICAL EVOLUTION MODEL WITH DUST

In this section, we describe the chemical evolution model implemented in the code GAMETE/QSODUST.

We will indicate with $M_{\rm ISM}$ the total mass in the ISM ($M_{\rm gas} + M_{\rm d}$) and with M_Z the total mass of metals (diffused in the gas phase and condensed into dust grains). At any given time, the mass of *gas-phase* metals is calculated as the difference between M_Z and $M_{\rm d}$ (with proper stoichiometric coefficients when we are interested in a particular gas-phase element). The variations in the total mass of gas, stars, metals and dust is followed in each progenitor halo of the hierarchical tree solving the following set of differential equations:

$$\frac{{\rm d}M_*(t)}{{\rm d}t} = {\rm nSFR(t)} - \frac{{\rm d}R(t)}{{\rm d}t}, \tag{15}$$

$$\frac{{\rm d}M_{\rm ISM}(t)}{{\rm d}t} = -{\rm nSFR(t)} + \frac{{\rm d}R(t)}{{\rm d}t} + \frac{{\rm d}M_{\rm inf}(t)}{{\rm d}t} - \frac{{\rm d}M_{\rm ej}(t)}{{\rm d}t}$$
$$- (1 - \epsilon_{\rm r})\frac{{\rm d}M_{\rm accr}(t)}{{\rm d}t}, \tag{16}$$

---

[4] The most massive stars exploding in an association will be very effective in destroying dust while sweeping up matter into a shell. Subsequent SNe will interact predominantly with the gas inside the shell and the shell itself and therefore do not contribute much to dust destruction. The expansion of the supershell is too slow to destroy much dust (e.g. Tielens 2005).

$$\frac{dM_Z(t)}{dt} = -Z_{ISM}(t)nSFR(t) + \frac{dY_Z(t)}{dt} + Z_{vir}(t)\frac{dM_{inf}(t)}{dt}$$
$$- Z_{ISM}(t)\frac{dM_{ej}(t)}{dt} - Z_{ISM}(t)(1-\epsilon_r)\frac{dM_{accr}(t)}{dt}, \quad (17)$$

$$\frac{dM_d(t)}{dt} = -Z_d(t)nSFR(t) + \frac{dY_d(t)}{dt} - \frac{M_d^{diff}(t)}{\tau_d} + \frac{M_d^{mc}(t)}{\tau_{acc}}$$
$$- Z_d(t)(1-\epsilon_r)\frac{dM_{accr}}{dt}, \quad (18)$$

where M_* and M_d are the total mass of stars and dust, $Z_{ISM}(t) = M_Z(t)/M_{ISM}(t)$ is the ISM metallicity, $Z_d(t) = M_d(t)/M_{ISM}(t)$ is the total dust abundance in the ISM and Z_{vir} is the metallicity of the infalling gas, namely of the hot gas at the virialization epoch. Its value corresponds to the metallicity of the external medium, that is, the ratio between the total mass of metals ejected by star-forming haloes and the mass of the diffused gas, not enclosed in collapsed objects (see SFS08 for details).

The new features of the code are summarized by (i) the evolution of dust described by equation (18); (ii) the term $(1-\epsilon_r)dM_{accr}/dt$ which accounts for the fraction, $1-\epsilon_r$, of the gas (metals and dust) that fuels BH growth via accretion; and (iii) the gas ejection rate $dM_{ej}(t)/dt = dM_{ej,SN}(t)/dt + dM_{ej,AGN}(t)/dt$ which includes both SN and AGN feedback.

Finally, the terms dR/dt, dY_Z/dt and dY_d/dt are the rates at which gas, heavy elements and dust, respectively, are returned to the ISM. The equations and grids of yields used to compute the gas- and metal-return fractions are the same as in SFS08 and V09: van den Hoeck & Groenewegen (1997) for AGB stars with initial metallicities $Z = (5 \times 10^{-2}, 0.2, 1)Z_\odot$ and masses 1–$8\,M_\odot$; Woosley & Weaver (1995) for SNe with initial masses 12–$40\,M_\odot$ at metallicities $Z = (0, 10^{-4}, 10^{-2}, 10^{-1}, 1)\,Z_\odot$; and Heger & Woosley (2002) for the PISNe assuming a reference progenitor mass of $200\,M_\odot$. The dust injection rate $dY_d(t)/dt$ is computed as in equation (12) of V09, including contributions from AGB stars, SNe and PISNe. We use the grids of Zhukovska, Gail & Trieloff (2008) for AGB stars with $0.8 \lesssim m \lesssim 8\,M_\odot$ at different metallicities; for SNe with progenitor mass of 12–$40\,M_\odot$[5] and metallicities $Z = (0, 10^{-4}, 10^{-2}, 10^{-1}, 1)Z_\odot$, we take the model by Bianchi & Schneider (2007) where grain condensation starts from seed clusters made of $\mathcal{N} \geq 2$ monomers with a sticking coefficient of $\alpha = 1$. We also assume that SNe explode in an ISM with a density of $\rho_{ISM} = 10^{-24}\,g\,cm^{-3}$, so that only 7 per cent of the initial dust formed in the ejecta survives the passage of the reverse shock. The resulting dust masses (10^{-3}–$10^{-1}\,M_\odot$ depending on the progenitor star initial mass and metallicity) are in agreement with the values inferred from observations of young SN remnants (e.g. Hines et al. 2004; Rho et al. 2008; Sandstrom et al. 2008; Rho et al. 2009). Finally, for PISNe, we adopt the dust yields computed by Schneider, Ferrara & Salvaterra (2004) for PISNe. As in V09, we extrapolate from the dust mass produced by the largest available AGB model ($7\,M_\odot$) and by the smallest SN progenitor ($12\,M_\odot$) to account for metal and dust production in the mass range 8–$11\,M_\odot$ for which the dust yields are not yet available in the literature. The grids of Zhukovska et al. (2008) are not computed at metallicity $Z < 5 \times 10^{-2}\,Z_\odot$; thus, we

Table 2. Model parameters. The models presented in this work are divided into two classes on the basis of the simulated SFH: quiescent-only (Q) and bursting (B) SF models. The numbers in the first column identify the efficiencies of SF in quiescent phases. The second column provides the value of σ_{burst} which determines the number, redshift distribution and intensity of the starbursts (B models only). The maximum starburst efficiency, $\epsilon_{burst,max}$, is given in the third column (B models only). Finally, the efficiency of gas accretion on to the central BH, α, and the efficiency of the AGN-driven wind, $\epsilon_{w,AGN}$, are shown in the last two columns.

Model	ϵ_{quies}	σ_{burst}	$\epsilon_{burst,max}$	α	$\epsilon_{w,AGN}$
Q1	0.045	–	–	190	5×10^{-3}
Q2	0.1	–	–	180	5×10^{-3}
Q3	1.0	–	–	350	5×10^{-3}
B1	6.7×10^{-3}	0.05	0.53	180	5×10^{-3}
B2	0.02	0.05	1.6	200	5×10^{-3}
B3	0.1	0.05	8.0	200	5×10^{-3}

have assumed that the dust mass produced by the AGB model at lower metallicities is the same as that at $Z = 5 \times 10^{-2}\,Z_\odot$.[6]

5 MODEL PARAMETERS

Our main aim is to investigate the effect of different SFHs in modelling the chemical properties of the host galaxy of the QSO J1148. The free parameters which determine the shape of the SFH are

(i) the SF efficiency, $f_*(z)$, which is determined by the choice of ϵ_{quies} and σ_{burst} (see equation 10),

(ii) the efficiency of the AGN-driven wind, $\epsilon_{w,AGN}$ (see equation 9), and

(iii) the efficiency of gas accretion on to the BHs, α (see equation 6).

The parameters which define the models considered in this work are summarized in Table 2 where the combinations of letters and numbers given in the first column identify each model.

These have been selected in order to reproduce the BH and total gas mass observed at $z = 6.4$. Given the uncertainties in the derivation of the stellar mass discussed in Section 2.2, we have not constrained evolutionary models in terms of the predicted final stellar mass. Indeed, by varying the global SF efficiency, $f_*(z)$, we explore the dependence of the final mass of metals and dust on the stellar mass and SFH, considering models which predict a stellar mass compatible with the value inferred by the observations ($3.9 \times 10^{10}\,M_\odot$, Walter et al. 2004), as well as models with higher stellar masses, closer to the value implied by the present-day M_{BH}–M_* relation ($\sim 10^{12}\,M_\odot$, see Fig. 3). The rate at which gas is converted into stars in quiescent (Q) models is regulated by the choice of the efficiency ϵ_{quies} given in the second column of the table (for these models $\epsilon_{burst} = 0$ in equation 10). In bursted (B) models, the frequency and amplitude of starbursts are regulated by the parameter σ_{burst}. The dependence on the choice of the latter parameter is investigated in Appendix A.

It has been shown that assuming an AGN wind efficiency $\epsilon_{w,AGN} = 5$ per cent, many observed properties of elliptical galaxies

[5] Dust and metal yields from Pop II/I stars with masses in the range 41–$100\,M_\odot$ are assumed to be zero. Indeed, it has been shown (e.g. Dwek 1998; Zhukovska et al. 2008, and reference therein) that such massive stars provide only a minor contribution to the total dust in the ISM with respect to that of AGB stars and core-collapse SNe.

[6] Note that this approximation may hold for carbon dust, but silicate dust production is likely to be significantly lower at low metallicity (see V09).
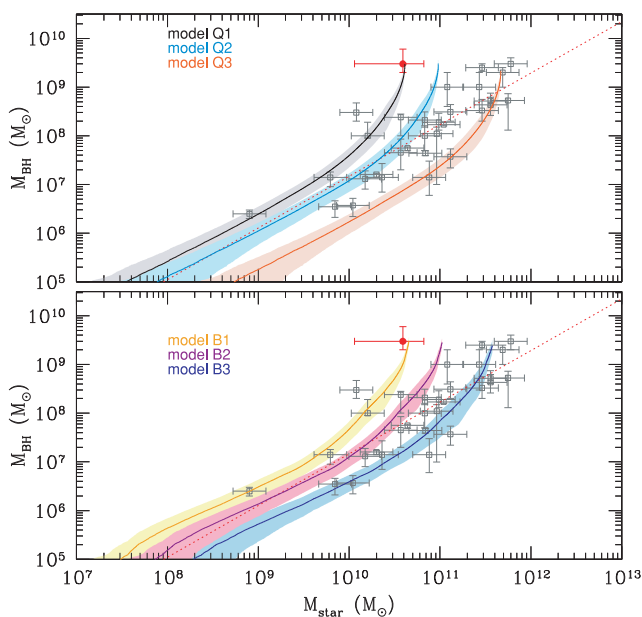
Figure 3. The evolution of the BH mass as a function of the stellar mass predicted by quiescent models (upper panel) and bursted models (lower panel). The open squared data points with error bars are from Marconi & Hunt (2003, table 1 in their work) and represent the $M_{BH} - M_*$ relation observed in the local Universe, with the empirical fit $M_{BH}/M_* \sim 0.002$ (dotted line) provided by the same authors. The filled circle shows the J1148 BH (Willott et al. 2003) and stellar masses (Walter et al. 2004) inferred from observations. For all models, the solid lines are averages over 50 merger tree realizations and the shaded areas represent 1σ dispersion.

as well as the observed $M_{BH} - \sigma$ correlation can be reproduced (see the discussion in Hopkins et al. 2006). Here, we follow a similar approach: in all the models presented here, we choose the parameters α and $\epsilon_{w,AGN}$ in order to reproduce the observed BH mass and to mimic a powerful AGN-driven wind which is able to sweep away enough gas from the host galaxy to reproduce the observed gas content and make the quasar optically visible, in its active phase, at $z = 6.4$. We set the parameter α in the range 180–350 to allow enough gas accretion to fuel the observed SMBH, and the wind efficiency, $\epsilon_{w,AGN}$, is chosen to regulate simultaneously the BH accretion, SF and gas ejection (to produce a global gas mass in agreement with the observational lower limit of Walter et al. 2004, see section 2.2).

Strictly speaking, the parameters listed in Table 2 are not independent. With higher SF efficiencies, f_*, less gas will be available for BH growth, thus requiring a higher BH accretion efficiency, α, in order to reproduce the observed BH mass. On the other hand, the higher is the BH accretion rate, the stronger is the AGN wind (and the earlier it affects the global gas content); thus, we need to set properly the coupling efficiency, $\epsilon_{w,AGN}$, to drive a gas outflow which expels the required amount of gas, but avoid a too-early decline of the SFR and BH accretion. Therefore, as it has emerged from the extensive exploration of the parameter space out of which the present models have been selected, the set of parameters that characterize each model are not unique. Given this degeneracy, we keep the value $\epsilon_{w,AGN} = 5 \times 10^{-3}$ fixed as we vary α, in order to easily compare the AGN feedback effects in different models and control the combined effect of BH accretion and AGN-driven gas outflow, in shaping the SFH. Unfortunately, the AGN-driven outflows are very difficult to observe if the quasar is in its active phase. As in the case of J1148, optically bright quasars outshine

their host galaxy and ionize the cold gas which is usually a tracer of the outflows. Thus, there are no observational constraints on the feedback process in such peculiar high-redshift objects.

6 RESULTS

In this section, we present the results of the semi-analytical hierarchical model GAMETE/QSODUST. We have performed 50 random realizations of the quasar hierarchical assembly (as explained in Section 3.1). Each of these merger histories allows us to predict a specific evolutionary path for the host galaxy chemical properties. However, to make the results and conclusions of this work independent of the hierarchical formation history, we will present the predicted evolution of the BH and galaxy properties averaging over all the 50 merger tree realizations.

6.1 BH evolution

As introduced in Section 2.2, we investigate the effects of the assumed SFH, considering models which predict stellar masses in agreement with the J1148 position on the $M_{BH} - M_*$ plane and with what would be implied if the system were to follow the observed local relation, taking into account the observational dispersion. Such models are shown in Fig. 3, which depicts the evolution on to the $M_{BH} - M_*$ plane predicted by quiescent models Q1, Q2 and Q3 (upper panel), and bursted models B1, B2 and B3 (lower panel). By construction, all models reproduce the observed J1148 SMBH mass but predict stellar masses increasing with f_*: low-f_* models (Q1 and B1) reproduce the M_* inferred from observations; high-f_* models (Q3 and B3) predict a final $M_{BH} - M_*$ correlation which is in agreement with the local observations (squared data points).

We note that, despite the different final stellar masses, all the models tend to approach the final value from the bottom. In other words, we find that in most of the models, the stellar bulge appears to evolve faster than the central BH ($M_* > 10^{10}\,M_\odot$ always for $M_{BH} \geq 10^8\,M_\odot$). This differs from the recent study by Lamastra et al. (2010) who predict an *evolution* with redshift of the $M_{BH} - M_*$ correlation, with higher z galaxies forming their nuclear BHs faster than their stellar mass. This may be due to the different physical descriptions of BH accretion and feedback, which, in the Lamastra et al. (2010) study, tend to enhance the accretion efficiency at high redshift.

For each model and at each redshift, we compute the *total* BH mass and accreted gas mass as the sum of all nuclear BHs and accretion rates hosted in each progenitor halo.[7] These are shown in Fig. 4. Due to the strong correlation between the parameters discussed above, the BH accretion rate (upper panels) and BH mass evolution (lower panels) have a negligible dependence on the particular model. At $z = 6.4$, we predict that J1148 has a BH mass of $\sim 3 \times 10^9\,M_\odot$ and accretes up to $\sim(20-30)\,M_\odot\,yr^{-1}$ of gas; in units of the Eddington rate, the predicted accretion rates are $\dot{M}_{BH}/\dot{M}_{Edd} \sim 0.3$–$0.45$ for all the models investigated. The thin line in the BH mass evolution (bottom panels) represents the final BH mass that would be produced only through BH mergers. It is

---

[7] Note that at each redshift/time-step of the simulation, each BH and its host halo are the progenitors of the final SMBH and its host galaxy, which, by construction, will form at $z = 6.4$. Therefore, at each redshift, the sum of all single-halo BH masses, as well as of the other quantities, such as the DM halo mass and the gas, star, metal and dust masses, is representative of the properties of the final halo at early times ($z > 6.4$).
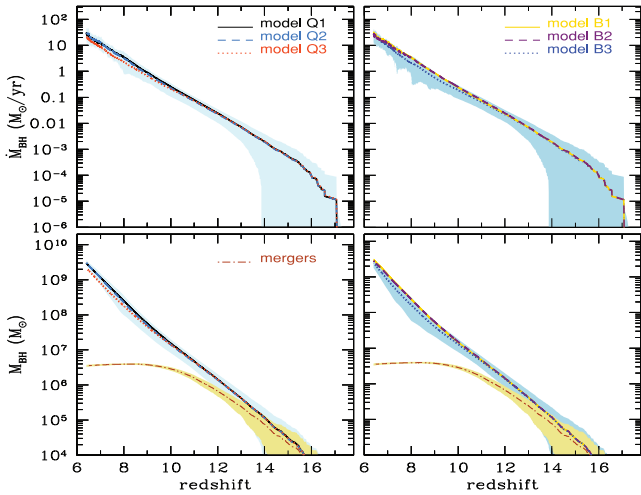
Figure 4. The BH accretion rate, $\dot{M}_{BH}$, and BH mass, M_{BH}, evolution as a function of redshift (upper and lower panels, respectively) in models Q (left-hand panels) and B (right-hand panels). The dot–dashed curves in the bottom panels represent the contribution to the BH mass by BH mergers.

clear from the figure that even if BH mergers are the main drivers for the early growth of the BH mass at $z > 11$, their contribution to the final BH mass at $z = 6.4$ is less than 1 per cent.

At $z > 11$, the dependence on the particular hierarchical formation history is stronger than at lower redshifts, as indicated by the larger shaded regions. Thus, differences between different realizations can influence only the early evolution of nuclear BHs. At $z \lesssim 11$, the main BH growth mechanism is gas accretion.

In Fig. 5, we explore, for a single merger history of model Q2, the dependence of the evolution of the BH mass on the assumed seed BH. We find that models with $M_{seed} \leq 10^3\,h^{-1}$ cannot reproduce the observed BH mass without increasing the accretion efficiency (α). On the other hand, for seed BHs with mass larger than $\sim 10^4\,M_\odot$, the BH accretion rate and BH mass at the final redshift $z = 6.4$ do
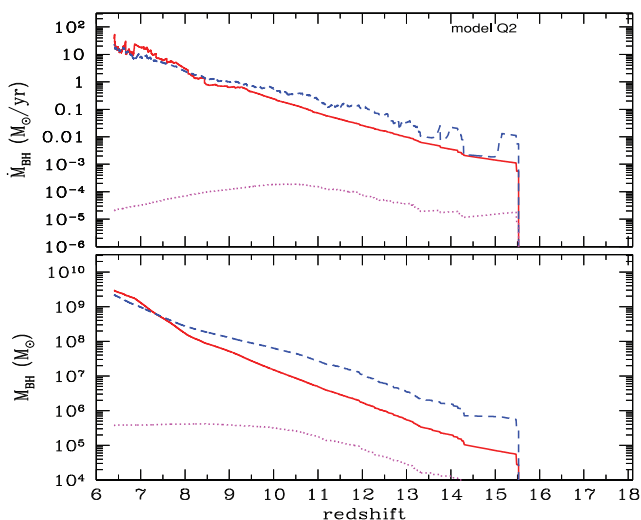

Figure 5. The BH accretion rate, $\dot{M}_{BH}$, and BH mass, M_{BH}, evolution as a function of redshift in model Q2 for different seed BH masses. The magenta (dotted), red (solid) and blue (dashed) lines show the results for a single merger tree realization, assuming seed BH masses of 10^3, 10^4 and $10^5\,h^{-1}\,M_\odot$, respectively.
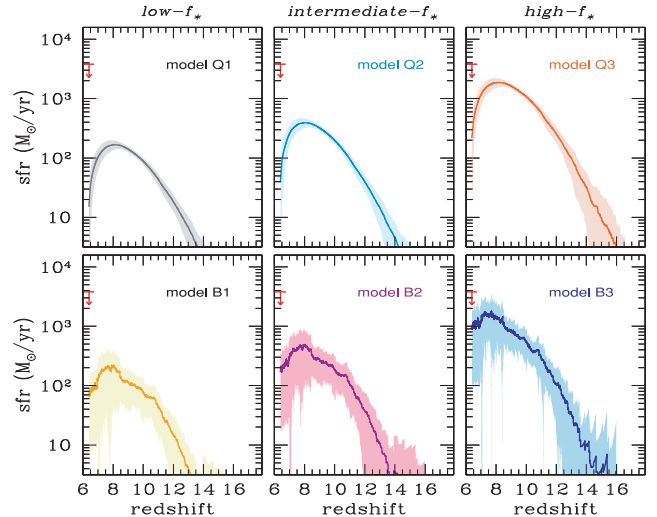

Figure 6. The SFHs of the host galaxy of the quasar J1148 in quiescent models Q1, Q2 and Q3 (upper panels, from the left-hand to right-hand side) and in bursted models B1, B2 and B3 (lower panels, from the left-hand to right-hand side). The arrow indicates the upper limit SFR inferred from the observation of J1148. The SFHs shown in this figure are obtained averaging over 50 random halo merger tree realizations and are shown together with the 1σ error represented by the shaded areas.

not depend much on the adopted seed. This is due to the interplay between Eddington-limited BH accretion and AGN feedback processes which efficiently regulate BH growth. These results justify the seed BH mass adopted in the models (see Section 3.3.1).

6.2 Star formation histories

The different SFHs produced by quiescent (Q1, Q2 and Q3) and bursted (B1, B2 and B3) SFH models are shown in Fig. 6 (upper and lower panels, respectively), with increasing global SF efficiencies, from *low* to *high* f_*.

As it can be seen from the figure, all SFHs peak at redshift ~ 8, with peak amplitudes increasing with f_*. The subsequent decrease is due to the effect of AGN feedback triggered by a large enough gas accretion rate on to the central BH. The galactic-scale wind expels gas from the halo (see Fig. 7), reducing the SF rate by a factor of ~ 2–10. The suppression of the SF rate is stronger in Q models where the rate of SF depends only on the available mass of gas at each redshift and does not depend on the merging haloes' mass ratio and redshift distribution. Indeed, such models are only mildly affected by variation in the different merger tree realizations, as also demonstrated by the narrow 1σ dispersion.

Conversely, in the B models, the available gas mass at each redshift, and thus the shape of the SFH, is determined by the enhanced starburst efficiency which depends on the parameter σ_{burst}. The number, intensity and redshift distribution of the starbursts strongly reflect the hierarchical merger history of the hosting DM halo. In fact, for the same set of parameters, each model shows a wide dispersion between the results obtained by individual merger histories, with their specific redshift distribution of major mergers which trigger the starbursts. The individual SFHs show very different features, such as the onset of starbursts or the redshift at which the last major merger occurs. This is reflected in the large 1σ dispersions which characterize B models.
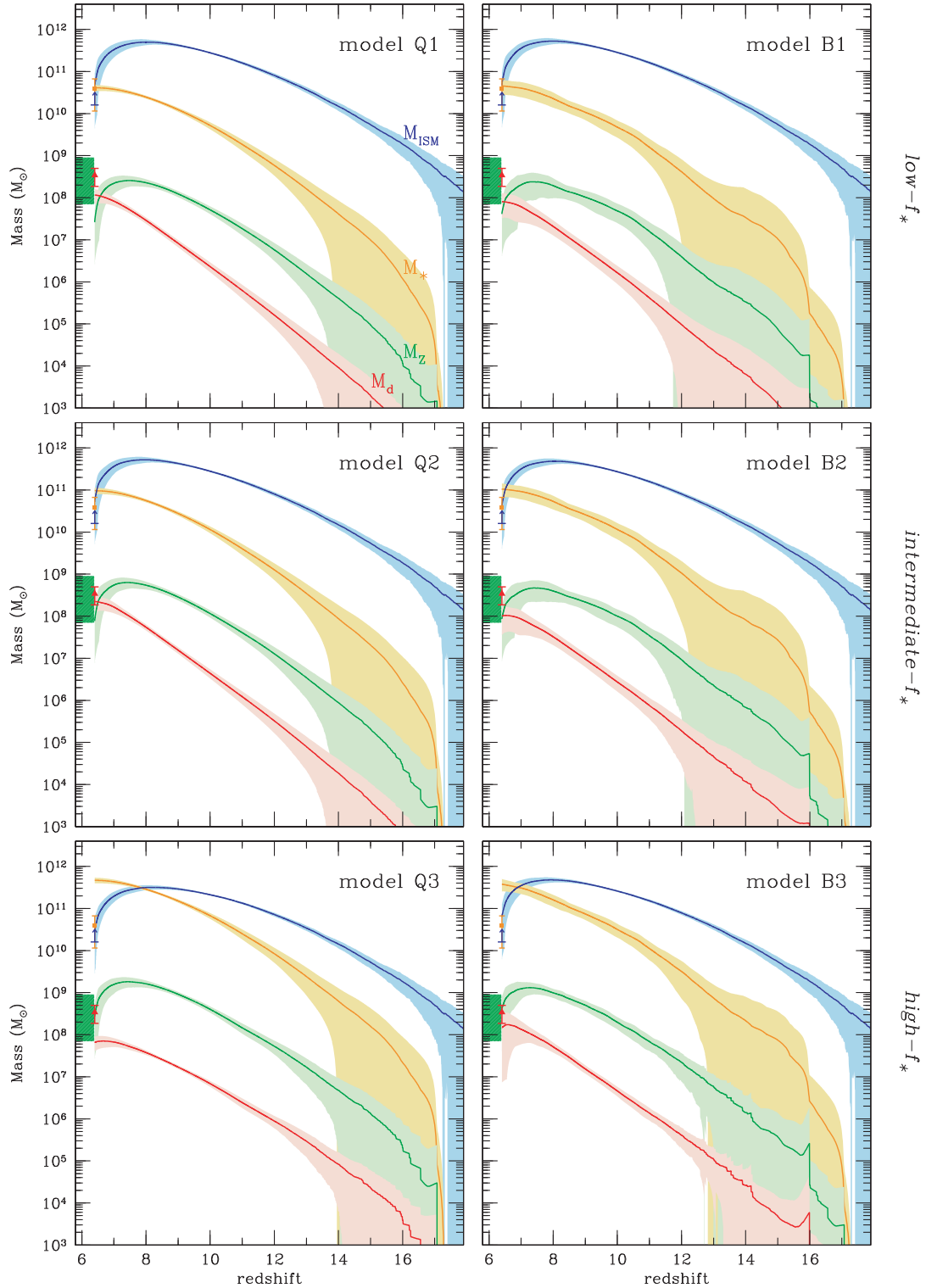
Figure 7. The ISM chemical evolution for the quasar J1148 host galaxy in different models. The lines show the redshift evolution of the average mass of gas, stars, metals and dust. Upper panels: low-f_* models Q1 (left-hand panel) and B1 (right-hand panel); middle panels: intermediate-f_* models Q2 (left-hand panel) and B2 (right-hand panel); lower panels: high-f_* models Q3 (left-hand panel) and B3 (right-hand panel). In all panels, the solid lines represent the average over 50 merger tree realizations and the shaded regions are the 1σ dispersion. The arrow is the lower limit to the gas mass inferred by observations. The circle indicates the final stellar mass with error bars accounting for the uncertainties on the estimates of the dynamical mass. The triangle shows the expected average dust mass with error bars accounting for the range of values given in the literature (see Table 1). Finally, the filled rectangle represents the estimated metallicity (see text).

We note that only model B2 and high-f_* models predict average SFRs at $z = 6.4$ in the range 200–900 $M_\odot$ yr^{-1}, in agreement with what inferred from observations of J1148, as discussed in Section 2.

6.3 Chemical evolution of the host galaxy

The evolution of the total mass of gas, stars, metals and dust (obtained, at each redshift, summing over all existing progenitors) for the host galaxy of J1148 predicted by the six models is shown in Fig. 7. We can immediately see that, independently of the assumed SFH, the mass of stars monotonically increases at decreasing redshift. On the contrary, the mass of gas and metals reaches a maximum value at $z \sim 8$ and then rapidly decreases as a consequence of the strong AGN feedback (see also Section 6.2). It is interesting to observe that, even for the evolution of the physical properties, B models (right-hand panels) show a higher dispersion among different hierarchical merger histories than Q models (left-hand panels). We can furthermore note that, except for the gas mass which is reproduced by construction, the final properties of the host galaxy strongly depend on the assumed SF efficiency, f_*.

Low-f_* models are the only ones which predict a final stellar mass in good agreement with that estimated from the observed dynamical and molecular gas masses of J1148 ($M_* \sim 4 \times 10^{10}\,M_\odot$). However, both fail to reproduce the final mass of dust and metals, which are underpredicted by a factor of 2–4. This result implies that, independently of the SFH, models which reproduce the observed stellar mass are not consistent with the observed chemical properties, at least if an ordinary IMF is assumed (see Section 6.4).

Intermediate-f_* models predict a final stellar mass ($M_* \sim 10^{11}\,M_\odot$) larger than observed but still inconsistent with the value expected from the local M_{BH}–M_* relation (see Fig. 3). As a consequence of the larger stellar mass, the total mass of metals produced increases and it is in (marginal) agreement with the observed value. The final dust mass is only reproduced by model Q2.

High-f_* models predict a final stellar mass in agreement with what expected from the local M_{BH}–M_* relation [$M_* \sim (4$–$5) \times 10^{11}\,M_\odot$] and reproduce the observed mass of metals. Note that, despite the large amount of metals available to accrete on to dust grains, the quiescent SFH model, model Q3, does not reproduce the observed mass of dust. This result, which is opposite to what found for the intermediate-f_* case, implies that an increase in the total stellar mass by a factor of 4–5 does not necessarily produce a similar enhancement in the total amount of dust. The origin of this behaviour will be discussed in the next section.

6.3.1 Evolution of dust

In this section, we investigate the evolution of the three components that contribute to the total dust content: (i) the mass of the dust grown in MCs from seed grains produced by stellar sources (*MC-grown dust*); (ii) the mass of the dust produced by AGB stars (*AGB dust*); and (iii) the mass of the dust formed in SN ejecta (*SN dust*). The evolution of each component along with the total mass of dust (solid red line) are shown in Fig. 8 for all the models.

It is clear from the figure that the dust grown in MCs from seed grains produced by stellar sources is the dominant dust component at $z < 10$. Indeed, the mass of dust contributed by stellar sources (green dot–dashed lines) is always subdominant at $z < 8$–10 and thus cannot reproduce the observed dust mass.

The evolution of the different components depends on the SFHs (bursted/quiescent) and SF efficiencies (low-/intermediate-/high-f_*
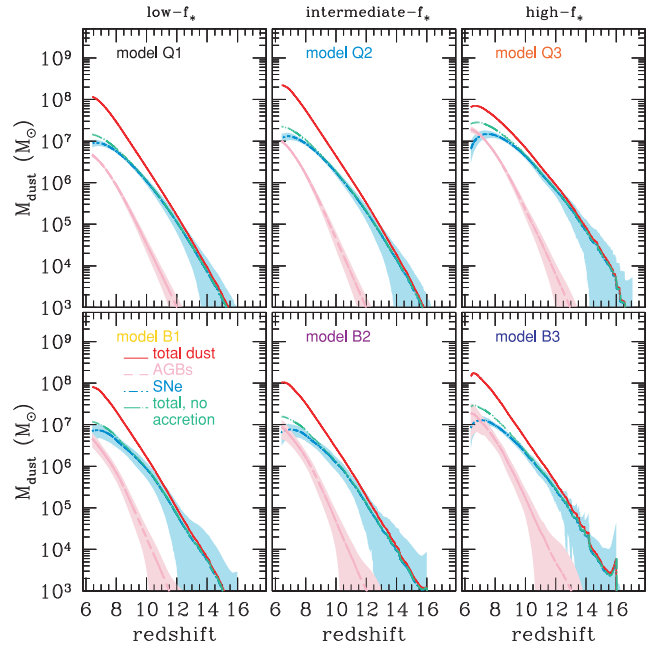

Figure 8. The evolution of individual dust components as a function of redshift for *low-f_** models Q1 and B1 (left-hand upper and lower panels, respectively), *intermediate-f_** models Q2 and B2 (middle upper and lower panels, respectively) and *high-f_** models Q3 and B3 (right-hand upper and lower panels, respectively). In all panels, the total dust mass (red lines) is compared with (i) the dust mass computed without the *MC-grown* dust contribution (green lines); (ii) the *SN-dust* components (cyan lines); and (iii) the *AGB-dust* components (pink lines). All lines are computed by averaging over 50 independent merger trees and the shaded regions represent the 1σ dispersions for SN- and AGB-dust components.

models). Focusing on stellar dust only, it is interesting to note that a factor of $\sim$10 increase in the final mass of stars (going from low- to high-f_* models) does not imply a similar increase in the final dust mass: the average dust mass produced by stellar sources (green lines) increases by less than a factor of 3 and it is almost independent of the SFH. Conversely, the relative importance of AGB stars and SNe depends both on the SFH and on the SF efficiency. In model B2 and high-f_* models, AGB stars dominate the stellar dust production in the last 150–200 Myr of evolution, after the peak of SF and when the effects of SN and AGN feedback lead to a strong reduction in the available gas mass. Interestingly, the mass of dust produced by AGB stars is found to increase in models with a higher SF efficiency, while a similar effect is not observed for SN dust. Indeed, at $z = 6.4$, the mass of SN dust in high-f_* models is comparable or smaller than in low- and intermediate-f_* models. This effect can be clarified by the following very simple analytic argument: assuming that SNe are the only dust producers, we can integrate equation (18) neglecting the last two terms and applying the instantaneous recycling approximation to obtain the 'effective' dust yield,

$$y_{d,SN}^{eff} = \frac{M_{dust,SN}}{M_*} \sim y_{d,SN} - Z_d(1 + \epsilon_d M_{swept} f_{SN} \mathcal{N}_{SN}), \qquad (19)$$

where $y_{d,SN}$ is the IMF-integrated yield of all stars with masses $\geq 8\,M_\odot$, $\mathcal{N}_{SN}$ is the number of SNe formed per unit mass of stars and the other symbols have been introduced in Section 3.3.4. Thus, as the dust-to-gas ratio, Z_d, grows in time, the effective dust yield decreases for the combined effect of astration and destruction due to SN shocks. The larger SF efficiencies in high-f_* models lead to

higher dust-to-gas ratios (rapid early dust enrichment and higher gas consumption) and are both characterized by lower effective dust yields with respect to models with lower f_*. For the typical dust yield adopted in this study (see Fig. 11 shown later), it is found that $y_{d,SN}^{eff} \sim 0$ when $Z_{d,cr} \sim 10^{-4}$. Thus, an order-of-magnitude estimate of the maximum mass of dust produced by SNe can be obtained as $Z_{d,cr} \times M_{gas,max} \sim 5 \times 10^7 \, M_\odot$ where we have assumed the maximum mass of gas shown in Fig. 7. This upper limit is consistent with the evolution shown in Fig. 8.

Since AGB stars evolve on longer time-scales, their net contribution is less affected by astration/destruction and the final mass of dust they produce increases with the increasing stellar mass (SF efficiency). However, this can only partly compensate for the reduced SN contribution, resulting in total stellar dust masses which vary by less than 30 per cent between different models and never exceed $3 \times 10^7 \, M_\odot$. We conclude that in all models, MC-grown dust is required in order to reproduce the observed dust mass. It was already suggested, although not confirmed, that the dust grown in MCs could have an important contribution to the observed dust mass in J1148, given the large molecular gas mass observed in this systems (Draine 2009). We find that the accretion of dust in MCs can easily increase the stellar dust mass by a factor of ~ 10 or more, reaching final values up to $\sim 2 \times 10^8 \, M_\odot$, the minimum required to match the observations.

Whether or not a model can reach this limit depends on the relative importance of the time-scales for dust destruction and accretion, τ_d and τ_{acc}. In Fig. 9, we show these two time-scales as a function of time for all the models discussed so far: in all cases, $\tau_{acc} \ll \tau_d$, with the exception of the latest stages of the evolution when, despite the decline in the supernova rate, gas and metal ejection due to AGN feedback conspires to decrease the destruction time-scale (less number of SNe are required to shock the remaining gas) and increase the accretion time-scale (less metal is available to be accreted on to dust grains, hence $f_{dep} \rightarrow 1$ in equation 12).

As expected, τ_d is progressively shorter in the models where the increase in the SF efficiency leads to larger SN rates. Thus, in models Q1, B1 and Q2, the final dust mass is controlled by accretion (limited by the available mass of metals), while in models B2, Q3 and B3, it is limited by destruction.
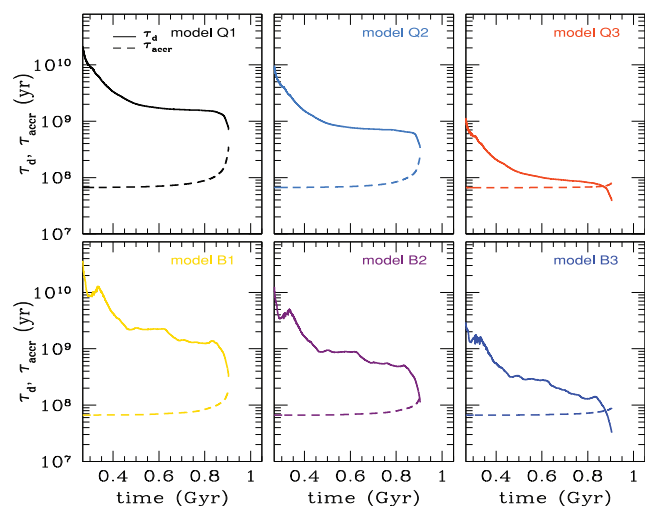

Figure 9. Time-evolution of the accretion (dashed lines) and destruction (solid lines) time-scales for quiescent models Q1, Q2 and Q3 (upper panels, from the left-hand to right-hand side) and bursted models B1, B2 and B3 (lower panels, from the left-hand to right-hand side).
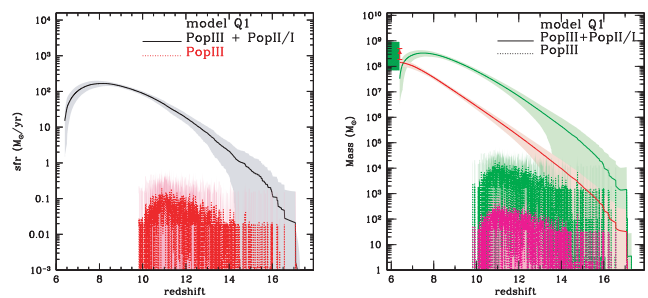
Figure 10. The contribution of the first stars to the chemical enrichment of the host galaxy ISM as predicted by model Q1. Left-hand panel: the SFH of Pop III stars (dotted line) as a function of redshift is compared with the total one (solid line). Right-hand panel: the mass of metals (green dotted line) and dust (magenta dotted line) produced by Pop III stars at each redshift is compared to the total one (solid line). The shaded areas represent the corresponding 1σ dispersion of each quantity.

6.3.2 The contribution of Population III stars to metal and dust enrichment

In this section, we analyse the contribution of Pop III stars to the metal and dust enrichment of the ISM of the QSO host galaxy. We discuss the results obtained in model Q1 since other models provide very similar conclusions.

The Pop III SFR as a function of redshift is shown in the left-hand panel of Fig. 10 (red dotted line with 1σ dispersion). The solid line represents the total (Pop III and Pop II/I) SFR (same as in the upper left-hand panel of Fig. 6). As it can be seen from the figure, the formation of Pop III stars is dominant only in the earliest phases of the evolution ($z > 16.5$) when the gas metallicity in progenitor star-forming haloes is subcritical ($Z < Z_{cr}$, see Section 3.2). In these haloes, the gas is promptly enriched by PISNe to metallicities $Z > Z_{cr}$, triggering the formation of lower mass stars; the formation of Pop III stars is still active down to redshift ~ 9.8. However, such starbursts typically occur in a small number of haloes at each redshift and the resulting Pop III SFR is orders of magnitude less efficient with respect to the total one.

The right-hand panel of Fig. 10 shows the mass of metals and dust contributed by Pop III stars at each redshift (green and magenta dotted lines, respectively) with the shaded areas indicating the corresponding 1σ dispersion. PISNe provide up to 100 per cent of the total mass of metals and dust at $z > 16$, but their contribution rapidly drops with time and at the final redshift, less than 5–10 per cent of the metal/dust mass is released by Pop III stars.

Thus, given their negligible contribution, we conclude that the choice of the characteristic mass for these stars does not influence the chemical evolution of the QSO host galaxy. This result is not surprising since, as already emphasized by Venkatesan, Schneider & Ferrara (2004), QSOs form in overdense regions of the Universe where the Pop III/Pop II transition occurs promptly and the enrichment is dominated by Pop II/I stars.

6.4 Chemical evolution with a top-heavy IMF

We have shown that low-f_* models, which reproduce the final stellar mass inferred from observations of J1148, fail to reproduce both the observed dust and the metal masses (see Fig. 7, upper panels). Depending on the adopted SFH, a factor of ~ 3 (model Q2, Fig. 7, middle left-hand panel) to ~ 10 (model B3, Fig. 7, lower right-hand panel) higher final stellar mass is required to reproduce the observed
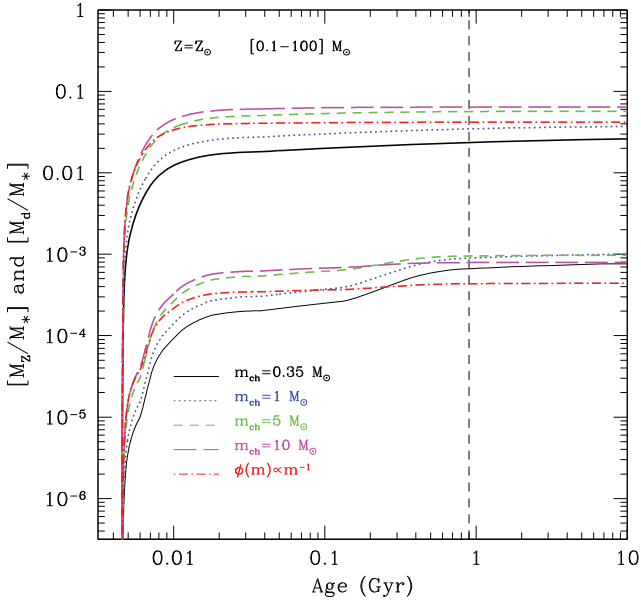
Figure 11. Evolution of the metal (upper lines) and dust (lower lines) yields as a function of stellar age. All stars are assumed to form in a single burst at $t = 0$ with solar metallicity, with a Larson IMF, with the characteristic masses $m_{ch} = 0.35, 1, 5$ and $10\,M_{\odot}$, and with a *flat* IMF (see text). The IMFs are normalized to unity in the mass range 0.1–100 $M_{\odot}$. The vertical line indicates the age of the Universe at $z = 6.4$.

chemical properties of J1148, if a Larson IMF with $m_{ch} = 0.35\,M_{\odot}$ is adopted.

In this section, we investigate how these results depend on the stellar IMF. Fig. 11 shows the evolution of the total metal (upper curves) and dust (lower curves) yields as a function of stellar age, assuming that all stars are formed in a single starburst at $t = 0$ with solar metallicity (see equation 1 in V09). Yields are computed for a Larson IMF with different characteristic masses, $m_{ch} = 0.35, 1, 5$ and $10\,M_{\odot}$, and for a *flat* IMF, $\phi(m) \propto m^{-1}$. The latter IMF has been proposed to reconcile predictions of semi-analytical models with the observed number counts of submillimetre galaxies at high redshift (e.g. Baugh et al. 2005, but see also Hayward et al. 2010).
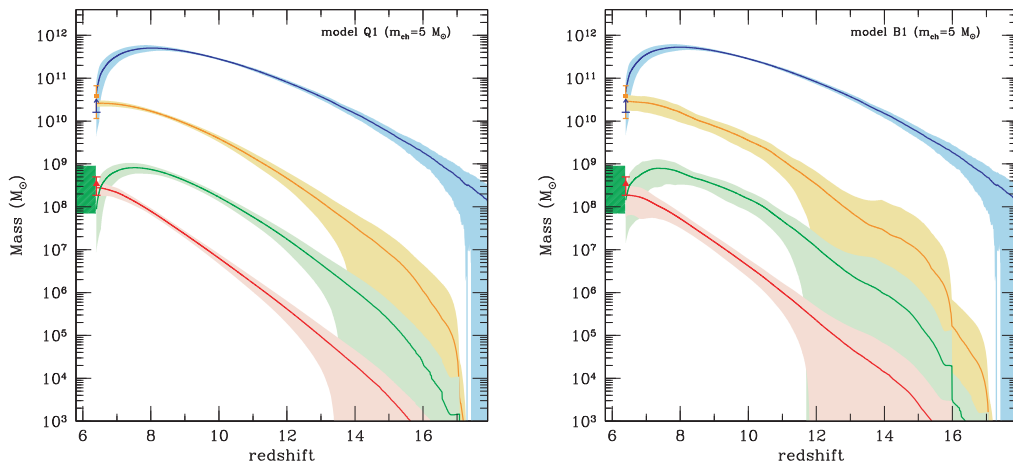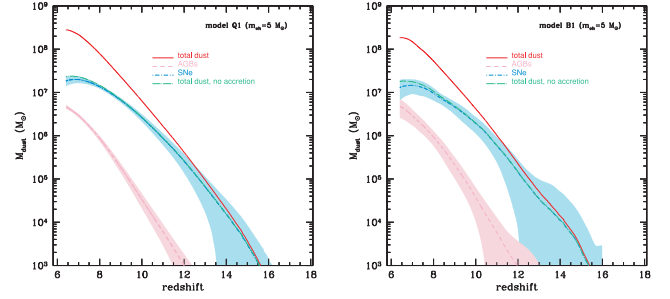

Figure 13. The same as in Fig. 8, but for low-f_* models with a top-heavy IMF (Larson IMF with $m_{ch} = 5\,M_{\odot}$).

IMFs are all normalized to unity in the mass range 0.1–100 $M_{\odot}$ and the vertical line indicates the age of the Universe at $z = 6.4$.

We find that a Larson IMF with $m_{ch} = 5\,M_{\odot}$ provides the most favourable conditions for larger amount of dust and metals to be contemporarily produced by a single stellar population: a factor of ~ 3 larger metal yield is produced when m_{ch} is increased from our standard value 0.35 $M_{\odot}$ to $m_{ch} = 5$–10 $M_{\odot}$. The highest amount of dust per unit stellar mass formed ($\sim 10^{-3}$) at $z = 6.4$ is obtained when a Larson IMF with $m_{ch} = 5\,M_{\odot}$ is adopted, which still includes a non-negligible contribution from AGB stars, comparable to that of SNe (see also V09).

Fig. 12 shows the resulting chemical properties for low-f_* models when a Larson IMF with $m_{ch} = 5\,M_{\odot}$ is adopted. With this *top-heavy* IMF, a factor of ~ 2–3 larger dust and metal masses at the final redshift $z = 6.4$ are produced compared to the same models with a *standard* IMF with $m_{ch} = 0.35\,M_{\odot}$ (Fig. 7, upper panels). A higher characteristic mass, m_{ch}, implies a larger number of intermediate- and high-mass stars. In fact, SN rates comparable to those found in intermediate-f_* models, which are characterized by a higher SF efficiency, are produced.

Since SNe have the dual role of both producing and destroying dust, the higher dust yield leads only to a moderate increase in the total mass of stellar dust. In Fig. 13, we show the time-evolution of individual dust components; the change in the IMF causes SNe to dominate stellar dust production at all redshifts. Yet, the total mass of stellar dust is still $\sim 2 \times 10^7\,M_{\odot}$, consistent with the

Figure 12. The same as in Fig. 7 but for *low-f_** models with a Larson IMF with $m_{ch} = 5\,M_{\odot}$.

argument[8] given by equation (19). The larger mass of metals available allows $\sim (2$–$3) \times 10^8 \, M_\odot$ of dust to grow in MCs; by the end of the simulation, an equilibrium in reached where $\tau_d \sim \tau_{acc}$; the onset of this equilibrium limits the mass of dust.

Thus, the observed chemical properties of J1148 seem to require either models with a factor of 3–10 larger stellar mass, which would shift this QSO close or on to the observed local stellar bulge–BH mass relation, or models with a non-standard IMF, in which stars form according to a Larson IMF with a high characteristic mass, $m_{ch} = 5 \, M_\odot$.

7 DISCUSSION

Several theoretical models aimed to investigate the formation and evolution of dust in high-redshift ($z > 5$) galaxies and quasars have been developed (e.g. Hirashita & Ferrara 2002; Morgan & Edmunds 2003; Dwek et al. 2007; V09; Dwek & Cherchneff 2011; Gall, Andersen & Hjorth 2010; Gall, Andersen & Hjorth 2011; Mattsson 2011). Models which reproduce the observed dust mass in J1148 using SNe as the primary sources require high dust yields (0.3–1 $M_\odot$), special SFHs (all stars formed in a starburst with age 0.3–100 Myr), top-heavy IMF and/or moderate dust destruction by interstellar shocks (Dwek et al. 2007; Gall et al. 2010, 2011; Dwek & Cherchneff 2011). The high dust yields required by these theoretical calculations are not supported by observations of local SNe (Wooden et al. 1993; Elmhamdi et al. 2003; Pozzo et al. 2004; Ercolano, Barlow & Stasinska 2007; Meikle et al. 2007; Kotak et al. 2009) and SN remnants. Among the latter class, the best studied source is Cas A which has been recently observed by *Spitzer* (Rho et al. 2008) and *Herschel* (Barlow et al. 2010), yielding an estimated dust mass in the range $2 \times 10^{-2} < M_{dust} < 7.5 \times 10^{-2} \, M_\odot$ (see, however, Dunne et al. 2009, who proposed the presence of $>0.1 \, M_\odot$ of dust in Cas A based on submillimetre polarization observations with the SCUBA).

Additional dust sources have been also proposed. In V09, we pointed out that AGB stars give an important contribution to the observed dust mass at $z > 6$ using a SFH for the host galaxy of J1148 as predicted by numerical simulations (Li et al. 2007). This finding has been recently confirmed by Dwek & Cherchneff (2011) and by Pipino et al. (2011); the latter also show that, on galactic scales, the dust produced by the AGN itself – a mechanism known as smoking QSOs (Elvis, Marengo & Karovska 2002) – is negligible when compared to that of stellar sources. Quantitative comparisons between various studies are difficult due to different prescriptions for computing dust formation and evolution (SFH, IMF, dust and metal yields, dust-destruction efficiencies). However, all the investigations published so far underline the important role played by the adopted SFH and IMF.

In this work, we have shown that MC-grown dust is the dominant component even at early cosmic epochs, $z > 6$, while stellar sources, SNe and AGB stars, cannot account for the total amount of dust observed in J1148. Their relative contribution is determined by the assumed SFH and IMF. This result differs from what was inferred by the simple toy-model presented in V09 for two main reasons: the peculiar input SFH and the close-box approximation made in V09. Specifically, the redshift of the last major burst of

SF and its intensity appear to provide the optimal conditions for dust production by stellar sources. In turn, our new results show the importance of a statistical analysis, where a sufficiently large sample of SFHs (merger tree realizations) can be investigated. In addition to that, galactic outflows determine the average ISM dust-to-gas ratio and have an indirect effect on the dust-destruction time-scales.

It has been shown in V09 that higher dust masses can be produced by decoupling the contribution of AGB stars from that of SNe. Indeed, we find that the largest stellar dust masses are found in some realizations of model B3 where the epoch and amplitude of the last major burst maximize dust production by AGB stars. Yet, when the average over many independent realizations is considered, the effect is partly washed out (see Appendix A).

Exploring different possible SFHs for the QSO host galaxy, we find that assuming a Larson IMF with $m_{ch} = 0.35 \, M_\odot$ the observed chemical properties (dust mass and gas metallicity) of J1148 seem to require a final stellar mass which is a factor of 3–10 higher than what inferred by observations of the dynamical and molecular gas masses. It is well known that observations of the dynamics and spatial distribution of molecular gas in J1148 (Walter et al. 2003), together with those which apply to a larger sample of QSOs with $5 < z < 6$ (Wang et al. 2010), seem to suggest a BH-to-stellar mass ratio which is 10–20 times higher than the present-day value, implying that the central BHs in these systems may assemble before their stellar bulge. Observations of dynamical and molecular gas are limited to the central 2.5 kpc of the host galaxy; a factor of 10 increase in the estimated stellar mass could be made consistent with the observations by simply assuming that the stellar bulge extends out to 25 kpc for realistic radial density distributions. More importantly, *the required stellar mass – based on chemical properties of the host galaxy – would shift the data point of J1148 on the BH–stellar mass relation much closer to the observed correlation in the present-day galaxies, at least within the observed scatter.*

Alternatively, all the observed properties of J1148 and its host galaxy can be reproduced if Pop II stars are assumed to form according to a Larson IMF with $m_{ch} = 5 \, M_\odot$, independently of the assumed SFH. Since SNe both form and destroy dust grains, the larger dust yield due to the higher SN rate leads only to a mild increase in the total dust mass produced by stellar sources. Yet, the larger metal yields lead to larger masses of gas-phase metals, which allow seed dust grains to efficiently grow in MCs. Indeed, physical conditions present in the ISM of QSO host galaxies at high z may favour a shift in the fragmentation mass scale of star-forming clouds, hence in the characteristic mass of the stellar IMF. Schneider & Omukai (2010) have studied the response of the thermal Jeans mass at cloud fragmentation to the joint effect of metal-line cooling, dust-cooling and the cosmic microwave background (CMB) in the ISM of high-redshift galaxies. They show that when $z \geq 5$ and the metallicity is $Z \geq 10^{-3} \, Z_\odot$, heating of dust grains by the CMB shifts the Jeans scale to larger masses. If no dust grains are present in star-forming clouds, the effect is even more dramatic and only massive and very massive stars are predicted to form (Jappsen et al. 2009; Smith et al. 2009). In addition to the effect of the CMB, MCs in circumnuclear starburst regions may be characterized by gas temperatures ~ 100 K and densities of a few times 10^5 cm^{-3}; under these conditions, numerical simulations predict that the resulting mass spectrum of gravitational condensations (a proxy to the IMF) is top-heavy, compared to that in the solar neighbourhood (Klessen, Spaans & Jappsen 2007).

In this study (as in V09), SN dust yields are obtained using one of the models proposed by Bianchi & Schneider (2007) where only

---

[8] It is important to note that although the SN dust yield, $y_{d,SN}$, is higher when $m_{ch} = 5 \, M_\odot$, the number of SNe formed per unit mass of stars, $\mathcal{N}_{SN}$, is also higher, resulting in a $Z_{d,cr}$ comparable to the value found for a standard IMF.

7 per cent of the dust formed in SN ejecta survives the passage of the reverse shock. According to this model, $\sim(0.5\text{–}5) \times 10^{-2} \, M_\odot$ of dust per SN is injected in the ISM (depending on the progenitor star mass and metallicity), in good agreement with the dust observed in young SN remnants. It is important to discuss how a different choice would affect the results presented in previous sections. Indeed, if we adopt an alternative model proposed by Bianchi & Schneider (2007), where the fraction of SN-condensed dust which is injected into the ISM is 20 per cent, we find that the final dust masses are similarly shifted upwards by a factor of ~ 3, bringing models Q1 and B1 in agreement with the observational data point. However, both models severely underpredict the mass of metals. Thus, although a higher SN dust yield leads to a larger total dust mass (closer to the observed value), a larger final stellar mass or a top-heavy IMF is still required to reproduce all the observed properties of J1148.

A final remark concerns the adopted prescription for the AGN feedback. Feruglio et al. (2010) have recently detected the broad wings of the CO line in Mrk 231, the closest known QSO, which has enabled to trace a giant molecular outflow of about $700 \, M_\odot \, \text{yr}^{-1}$; the inferred kinetic energy in the molecular outflow is 1.2×10^{44} erg s^{-1}, corresponding to a few per cent of the AGN bolometric luminosity (5×10^{45} erg s^{-1}). This is consistent with what we find in our simulated models. In fact, the formulation adopted for the BH accretion rate ensures that BH feedback is active over almost the entire lifetime of the host halo (since the computed rate is almost always above the critical threshold), resulting in an efficient gas ejection at lower redshift ($z < 7\text{–}8$) when the BH mass and its gas accretion rate are higher. This, in turn, is regulated by the choice of the parameters α and $\epsilon_{w,AGN}$. However, it is important to note that the relative role of starbursts and AGN activity in regulating/quenching SF and BH growth, as well as the mechanisms (energy/momentum deposition) driving these feedback processes, is still largely debated (see e.g. Debuhr et al. 2010; Hopkins 2011; Hopkins, Quataert & Murray 2011, for a different view).

8 SUMMARY AND CONCLUSIONS

Here we have presented a semi-analytical model which allows to (i) model the evolution of a QSO host galaxy and its central SMBH, predicting a range of possible SFHs; and (ii) explore the relative importance of stellar sources of dust (SNe and AGB stars) and of the dust grown in MCs at these early cosmic epochs. GAMETE/QSODUST follows the build-up of the central SMBH through mergers and gas accretion, starting from seed BHs at very high redshifts. The corresponding assembly of the host galaxy is followed in a self-consistent way and the co-evolution of these two fundamental components is controlled by AGN feedback in the form of a galactic-scale wind, assuming that 0.5 per cent of the rest-mass energy of the gas accreted on to the BH is thermally coupled to the ISM. We have performed 50 random hierarchical merger histories of a $10^{13}\text{-}M_\odot$ DM halo, which is believed to host a $>10^9 \, M_\odot$ SMBH, through a binary Monte Carlo algorithm with mass accretion based on the EPS theory.

Metal and dust enrichment is followed by evolving all progenitor galaxies on the corresponding stellar lifetimes, considering the contribution from Pop III (PISNe) and Pop II stars (AGB stars and SNe), and the subsequent dust grain processing (destruction and growth) in the ISM. Metal and dust yields are taken from theoretical models for stellar nucleosynthesis and dust nucleation in SN ejecta and AGB stellar atmospheres. Different SFHs for the QSO host galaxy have been explored: in quiescent models, the efficiency

of SF is independent of the galaxy mergers' mass ratio, while in bursted models, the SF efficiency is enhanced during major mergers between progenitor galaxies. The free parameters of the models, namely the efficiency of SF, BH accretion and AGN-driven wind, have been chosen to reproduce the BH and gas mass inferred from observations of J1148 at $z = 6.4$.

The main results of this study can be summarized as follows:

(i) The chemical properties of the host galaxies of high-z QSOs are a powerful probe of their past evolution. The dust mass produced by stars depends on the shape of the SFH, which is controlled by the evolution of the gas content through mergers and outflows driven by SNe and the AGN. The total mass of metals is a tracer of the integrated SFH (total stellar mass) and it is sensitive to the strength and frequencies of metal-rich outflows.

(ii) Pop III stars give a negligible contribution to the chemical enrichment of the ISM. In fact, the large metal and dust yields expected from theoretical models of PISNe lead to rapid enrichment of the ISM to metallicities $Z \geq Z_{cr} = 10^{-6}\text{–}10^{-4} \, Z_\odot$ in progenitor galaxies of the final galaxy host, enabling the formation of Pop II/I stars.

(iii) If Pop II/I stars form with a *standard IMF* and a characteristic stellar mass of $m_{ch} = 0.35 \, M_\odot$, as in the present-day Universe, the final masses of metals and dust are lower than observed. Depending on the adopted SFH, a final stellar mass which is a factor of 3–10 larger than the value inferred from observations of the dynamics and spatial distribution of the molecular gas content of J1148 (Walter et al. 2003) is required. The required stellar mass would shift the position of J1148 on to the locally observed correlation between the SMBH and stellar bulge masses, at least within the observed scatter.

(iv) If Pop II/I stars form with a *top-heavy IMF* and a characteristic stellar mass of $m_{ch} = 5 \, M_\odot$, then the observed chemical properties can be reconciled with the inferred stellar mass. The physical conditions of star-forming regions in these high-z systems may in fact suppress fragmentation, due to higher temperatures in MCs and heating of dust grains, favouring the formation of larger stellar masses.

(v) A statistical analysis of the SFHs, with many independent hierarchical merger trees of the DM halo hosting J1148, has allowed us to conclude that although SNe dominate the early dust enrichment, AGB stars contribute at $z < 8\text{–}10$; the latter contribution depends on the shape of the SFH and on the adopted IMF for Pop II/I stars.

(vi) We find that stellar sources produce a total dust mass which never exceeds $\sim(2\text{–}3) \times 10^7 \, M_\odot$; in fact, unless the redshift and intensity of the last major burst of SF allow to efficiently decouple the contribution of SNe and AGB stars, the effective dust yield is progressively reduced due to the joint effect of astration and dust destruction in the ISM by SN shocks. This conclusion is independent of the adopted stellar IMF but depends on the adopted stellar dust yields.

(vii) In all the models we have investigated, the final dust mass can be reconciled with the observed value, $M_{dust} = (2\text{–}6) \times 10^8 \, M_\odot$, via grain growth in MCs, which appears to be important even at these high redshifts, consistent with the large molecular gas mass observed in J1148. The final mass of dust is thus controlled by two fundamental time-scales: the time-scale for grain growth (which becomes progressively longer due to rapid depletion of metals in dust grains) and the time-scale for the dust destruction by SN shocks (which depends on the SFH through both gas consumption/ejection and the SN rate).

REFERENCES

Baker J. G., Centrella J., Choi D., Koppitz M., van Meter J., 2006, Phys. Rev. Lett., 96, 111102
Barlow M. J. et al., 2010, A&A, 518, L138
Barth A. J., Martini P., Nelson C. H., Ho L. C., 2003, ApJ, 594, L95
Baugh C. M., Lacey C. G., Frenk C. S., Granato G. L., Silva L., Bressan A., Benson A. J., Cole S., 2005, MNRAS, 356, 1191
Becker G. D., Sargent W. L. W., Rauch M., Simoncoe R. A., 2006, ApJ, 640, 69
Beelen A., Cox P., Benford D. J., Dowell C. D., Kovacs A., Bertoldi F., Omont A., Carilli C. L., 2006, ApJ, 642, 694
Begelman M. C., Volonteri M., Rees M. J., 2006, MNRAS, 370, 289
Bertoldi F., Carilli C. L., Cox P., Fan X., Strauss M. A., Beelen A., Omont A., Zylka R., 2003, A&A, 406, L55
Bianchi S., Schneider R., 2007, MNRAS, 378, 973
Bianchi S., Schneider R., Valiante R., 2009, in Henning T., Grün E., Steinacker J., eds, ASP Conf. Ser. Vol. 414, Cosmic Dust - Near and Far. Astron. Soc. Pac., San Francisco, p. 65
Bondi H., Hoyle F., 1944, MNRAS, 104, 273
Booth C. M., Schaye J., 2009, MNRAS, 398, 53
Bromm V., Loeb A., 2003, ApJ, 596, 34
Campanelli M., Lousto C., Marronetti P., Zlochower Y., 2006, Phys. Rev. Lett., 96, 111101
Cardelli J. A., Clayton G. C., Mathis J. S., 1989, ApJ, 345, 245
Charmandaris V., Uchida K. I., Weedman D., Herter Y., Houck J. R., Telpiz H. I., Armus L., Brandl B. R., 2004, ApJS, 154, 142
Ciotti L., Ostriker J. P., Proga D., 2009, ApJ, 699, 89
Ciotti L., Ostriker J. P., Proga D., 2010, ApJ, 717, 708
Cole S., Lacey C. G., Baugh C. M., Frenk C. S., 2000, MNRAS, 319, 168
Cox T. J., Jonsson P., Somerville R. S., Primack J. R., Dekel A., 2008, MNRAS, 384, 386
Daddi E., Elbaz D., Walter F., Bournaud F., Salmi F., Carilli C., Dannerbauer H., Dickenson M., 2010, ApJ, 714, 118
Dasyra K. M., Yacconi L. J., Davies R. I., Naab T., Genzel R., Lutz D., Sturm E., Baker A. J., 2006, ApJ, 651, 835
Debuhr J., Quataert E., Ma C. P., Hopkins F., 2010, MNRAS, 406, L55
Di Matteo T., Springel V., Hernquist L., 2005, Nat, 433, 604
Di Matteo T., Colberg J., Springel V., Hernquist L., 2008, ApJ, 676, 33
Draine B. T., 1990, in Blitz L., ed., ASP Conf. Ser. Vol. 12, The Evolution of the Interstellar Medium. Astron. Soc. Pac., San Francisco, p. 193
Draine B. T., 2009, in Henning T., Grün E., Steinacker J., eds, ASP Conf. Ser. Vol. 414, Cosmic Dust Near and Far. Astron. Soc. Pac., San Francisco, p. 453
Dunne L., Eales S., Edmunds M., Ivison R., Alexander P., Clements D. L., 2000, MNRAS, 315, 115
Dunne L. et al., 2009, MNRAS 394, 1307
Dwek E., 1998, ApJ, 302, 363
Dwek E., Scalo J. M., 1980, ApJ, 239, 193
Dwek E., Cherchneff I., 2011, ApJ, 727, 63
Dwek E., Galliano F., Jones A. P., 2007, ApJ, 662, 927
Ellison S. L., Patton D. R., Simard L., McConnachie A. W., Baldry I. K., Mendel J. T., 2010, MNRAS, 407, 1514
Elmhamdi A. et al., 2003, MNRAS, 338, 939
Elvis M., Marengo M., Karovska M., 2002, ApJ, 567, L107

Ercolano B., Barlow N., Stasinska G., 2007, MNRAS, 375, 753
Fan X. et al., 2004, AJ, 128, 515
Fan X. et al., 2003, AJ, 125, 1649
Feruglio C., Maiolino R., Piconcelli E., Menci N., Aussel H., Lamastra A., Fiore F., 2010, A&A, 518, L155
Gall C., Andersen A. C., Hjorth J., 2010, A&A, 528, 13
Gall C., Andersen A. C., Hjorth J., 2011, A&A, 528, 14
Gallerani S., Maiolino R., Juarez Y., Nagao T., Marconi A., Bianchi S. et al., 2010, A&A, 523, 85
Genzel R., Tacconi L. J., Rigopoulou D., Lutz D., Tecza M., 2001, ApJ, 563, 527
Haring N., Rix H. W., 2004, ApJ, 604, L89
Hayward C. C., Narayanan D., Jonsson P., Cox T. J., Keres D., Hopkins P. F., Hernquist L., 2011, in Treyer M., Wyder T., Neill J. D., Seibert M., Lee J. C., eds, ASP Conf. Ser. Vol. 440, UP 2010: Have observations revealed a variable upper end of the initial mass function? Astron. Soc. Pac., San Francisco, p. 369
Heger A., Woosley S. E., 2002, ApJ, 567, 532
Hines D. C. et al., 2004, ApJS, 154, 290
Hirashita H., 1999, A&A, 344, L87
Hirashita H., Ferrara A., 2002, MNRAS, 337, 921
Hopkins P. F., 2011, preprint (arXiv:1101.4230)
Hopkins P. F., Hernquist L., Cox T. J., Di Matteo T., Robertson B., Springel V., 2006, ApJS, 163, 1
Hopkins P. F., Quataert E., Murray N., 2011, preprint (arXiv:1101.4940)
Hoyle F., Lyttleton R. A., 1939, Proc. Camb. Philos. Soc., 35, 405
Jappsen A. K., Mac Low M. M., Glover S. C. O., Klessen R. S., Kitsionas S., 2009, ApJ, 694, 1161
Jiang L. et al., 2010, Nat, 464, 380
Jones A. P., Tielens A. G. G. M., Hollenbach D. J., 1996, ApJ, 469, 740
Juarez Y., Maiolino R., Mujica R., Pedani M., Marinoni S., Nagao T., Marconi A., Olive E., 2009, A&A, 494, 25
Kennicutt R., 1998, ApJ, 498, 541
Klessen R. S., Spaans M., Jappsen A. K., 2007, MNRAS, 374, L29
Kotak R. et al., 2009, ApJ, 704, 306
Lacey C., Cole S., 1993, MNRAS, 262, 627
Lamastra A., Menci N., Maiolino R., Fiore F., Merloni A., 2010, MNRAS, 405, 29
Li Y. et al., 2007, ApJ, 665, 187
Li Y. et al., 2008, ApJ, 678, 41
McLure R. J., Jarvis M. J., 2002, MNRAS, 337, 109
Maiolino R., Schneider R., Oliva E., Bianchi S., Ferrara A., Mannucci F., Pedani M., Roca Sogorb M., 2004, Nat, 431, 533
Maiolino R. et al., 2005, A&A, 440, L51
Maiolino R. et al., 2006, Mem. Soc. Astron. Ital., 77, 643
Marchenko S. V., 2006, in Lamers H. J. G. L. M., Langer N., Nugis T., Annuk K., eds, ASP Conf. Ser. Vol. 353, Stellar Evolution at Low Metallicity: Mass Loss, Explosions, Cosmology. Astron. Soc. Pac., San Francisco, p. 299
Marconi A., Hunt L. K., 2003, ApJ, 589, L21
Marconi A., Axon D. J., Maiolino R., Nagao T., Pastorini G., Pietrini P., Robinson A., Torricelli G., 2008, ApJ, 678, 693
Matsuoka K., Nagao T., Maiolino R., Marconi A., Taniguchi Y., 2009, A&A, 503, 721
Mattsson L., 2011, MNRAS, 414, 781
McKee C., 1989, in Allamandola L. J., Tielens A. G. G. M., eds, Proc. IAU Symp. 135, Interstellar Dust. Kluwer Academic Publishers, Dorchester, p. 431
Meikle W., Mattila S., Pastorello A., Gerardy C., Kotak R., Sollerman J., Van Dyk S. D., Farrah D., 2007, ApJ, 665, 608
Merloni A., Heinz S., 2008, MNRAS, 388, 1011
Michalowski M. J., Murphy E. J., Hjorth J., Watson D., Gall C., Dunlop J. S., 2010, A&A, 522, 15
Mihos J. C., Hernquist L., 1996, ApJ, 464, 641
Morgan H. L., Edmunds M. G., 2003, MNRAS, 343, 427
Nagao T., Marconi A., Maiolino R., 2006, A&A, 447, 157
Nozawa T., Kozasa T., Habe A., 2006, ApJ, 648, 435

Nozawa T., Kozasa T., Habe A., Dwek E., Umeda H., Tominaga N., Maeda K., Nomoto K., 2007, ApJ, 666, 955

Padovani P., Matteucci F., 1993, ApJ, 416, 26

Pei Y., 1992, ApJ, 395, 130

Pentericci L. et al., 2002, AJ, 123, 2151

Perley D. et al., 2010, MNRAS, 406, 2473

Pipino A., Fan X. L., Matteucci F., Calura F., Silva L., Granato G., Maiolino R., 2011, A&A, 525, 61

Pozzo M., Meikle W. P. S., Fassia A., Geballe T., Lundqvist P., Chugai N. N., Sollerman J., 2004, MNRAS, 352, 457

Priddey R. S., Isaac K. G., McMahon R. G., Omont A., 2003, MNRAS, 338, 1183

Raiteri C. M., Villata M., Navarro J. F., 1996, A&A, 315, 105

Rho J., Kozasa T., Reach W. T., Smith J. D., Rudnick L., DeLaney T., Ennis J. A., Gomez H., 2008, ApJ, 673, 271

Rho J. et al., 2009, in Henning T., Grün E., Steinacker J., eds, ASP Conf. Ser. Vol. 414, Cosmic Dust - Near and Far. Astron. Soc. Pac., San Francisco, p. 22

Robson I., Priddey R. S., Isaak K. G., McMahon R. G., 2004, MNRAS, 351, L29

Salvadori S., Schneider R., Ferrara A., 2007, MNRAS, 381, 647 (SSF07)

Salvadori S., Ferrara A., Schneider R., 2008, MNRAS, 386, 348 (SFS08)

Sandstrom K., Bolatto A., Leroy A., Stanimirovic S., Simon J. D., Staveley-Smith L., Shah R., 2008, in Chary R. R., Teplitz H. I., Sheth K., eds, ASP Conf. Ser. Vol. 381, Infrared Diagnostics of Galaxy Evolution. Astron. Soc. Pac., San Francisco, p. 268

Schmidt M., Schneider D. P., Gunn J. E., 1995, AJ, 110, 68

Schneider R., Omukai K., 2010, MNRAS, 402, 429

Schneider R., Ferrara A., Salvaterra R., 2004, MNRAS, 351, 1379

Shakura N. I., Sunyaev R. A., 1973, A&A, 24, 337

Shankar F., 2009, New Astron. Rev., 53, 57

Sijacki D., Springel V., di Matteo T., Hernquist L., 2007, MNRAS, 380, 877

Silk J., Rees M. J., 1998, A&A, 31, L1

Smith B. D., Turk M. J., Sigurdsson S., O'Shea B. W., Norman M. L., 2009, ApJ, 691, 441

Somerville R. S., Hopkins P. F., Cox T. J., Robertson B. E., Hernquist L., 2008, MNRAS, 391, 481

Springel V., Di Matteo T., Hernquist L., 2005, MNRAS, 361, 776

Stratta G., Maiolino R., Fiore F., D'Elia V., 2007, ApJ, 661, L9

Tacconi L., Genzel R., Lutz D., Rigopoulou D., Baker A. J., Iserlohe C., Tecza M., 2002, ApJ, 580, 73

Tanaka T., Haiman Z., 2009, ApJ, 696, 1798

Tielens A. G. G. M., 1998, ApJ, 499, 267

Tielens A. G. G., 2005, The Physics and Chemistry of the Interstellar medium. Cambridge Univ. Press, Cambridge

Valiante R., Schneider R., Bianchi S., Andersen A. C., 2009, MNRAS, 397, 1661 (V09)

van den Hoek L. B., Groenewegen M. A. T., 1997, A&AS, 123, 305

Venkatesan A., Schneider R., Ferrara A., 2004, MNRAS, 349, L43

Vestergaard M., 2002, ApJ, 571, 733

Volonteri M., Natarajan P., 2009, MNRAS, 400, 1911

Volonteri M., Rees M. J., 2006, ApJ, 650, 669

Volonteri M., Haardt F., Madau P., 2003, ApJ, 582, 559

Watter F., Bertoldi F., Carilli C., Cox P., Lo K. Y., Neri R., Fan X., Omont A., Strauss M. A., Menten K. M., 2003, Nat, 424, 406

Walter F., Carilli C., Bertoldi F., Menten K., Cox P., Lo K. Y., Fan X., Strauss M. A., 2004, ApJ, 615, L17

Wang R. et al., 2008, ApJ, 687, 848

Wang R. et al., 2010, ApJ, 714, 699

Weingartner J. C., Draine B. T., 2001, ApJ, 548, 296

Willott C. J., McLure R. J., Jarvis M. J., 2003, ApJ, 587, L15

Wooden D. H., Rank D. M., Bregman J. D., Witteborn F. C., Tielens A. G., Cohen M., Pinto P. A., Axelrod T. S., 1993, ApJS, 88, 477

Woods D. F., Geller M. J., 2007, ApJ, 134, 527

Woosley S. E., Weaver T. A., 1995, ApJ, 101, 181

Wyithe J. S., Loeb A., 2003, ApJ, 595, 614

Zhukovska S., Gail H. P., Trieloff M., 2008, A&A, 479, 453

APPENDIX A: DEPENDENCE ON THE STARBURST FREQUENCY

With the aim of investigating the dependence of our results on the number and intensity of starbursts, we have explored two additional high-f_* SFHs, models B4 and B5 (see Table A1). These models predict a total stellar mass comparable to model B3 but with increasing values of σ_{burst} which imply SFHs characterized by an increasing number of (less efficient) bursts of SF. The resulting average SFHs are shown in Fig. A1 (thick lines and corresponding 1σ dispersion). The two SFH models have progressively less intense but more frequent bursts with respect to model B3. These differences are particularly evident when we compare the predictions of a single merger tree realization; the thin lines in Fig. A1 show the predicted SFHs in models B3–B5 for the same merger tree realization. Comparing with the corresponding thick lines in each panel, which represent the average SFH over 50 merger tree realizations, it becomes clear how the averaging procedure partly cancels the redshift-dependent effects.

The quasar host chemical evolution predicted by the additional models presented here, B4 and B5, is shown in Fig. A2. Even if the evolution at the highest redshifts is (slightly) different (the predicted masses are slightly higher and the curves are progressively smoother), the final masses of gas, stars and metals are very similar to what predicted by model B3 (lower right-hand panel in Fig. 7). On the other hand, we find that model B4 is in agreement with the observed dust mass within the 1σ dispersion on the average evolution (i.e. at least in one of the 50 merger histories the associated SFH is able to reproduce the observed properties of the quasar host), whereas model B5, which is characterized by a SFH with less intense and more frequent bursts, is not able to reproduce the observed dust mass.

Table A1. Model parameters of the two additional bursted SFH models B4 and B5. Column descriptions are the same as in Table 2.

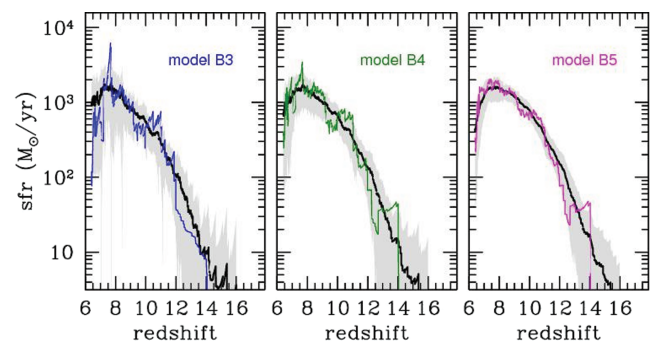| Model	ϵ_{quies}	σ_{burst}	$\epsilon_{burst,max}$	α	$\epsilon_{w,AGN}$
B4	0.1	0.1	4.0	233	5×10^{-3}
B5	0.1	0.25	1.6	250	5×10^{-3}

Figure A1. SFHs in high-f_* models B3, B4 and B5 for a single merger tree realization (thin lines). The panels show the effects of different values of the parameter σ_{burst}: 0.05 (model B3, left-hand panel), 0.1 (model B4, middle panel) and 0.25 (model B5, right-hand panel). The thick solid lines refer to the average over 50 merger tree realizations (see text).
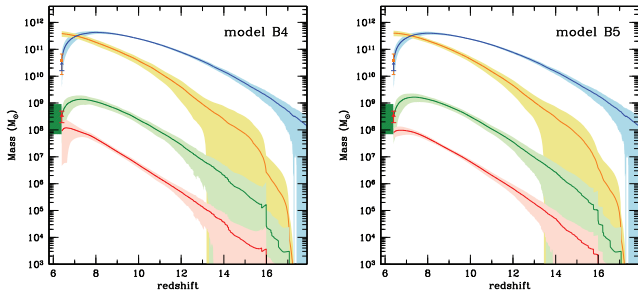
Figure A2. Evolution of the chemical properties (gas, stars, metals and dust) for bursted SF models B4 and B5. The line colours and observational constraints are the same as in Fig. 7.

This analysis shows the following:

(i) By averaging the results over a set of merger tree realizations, the specific features of each single SFH, such as the number, intensity and redshift distribution of starbursts, and the intensity and position of the burst triggered by the last major merger, are partly washed out.

(ii) An increasing number of starbursts do not produce a larger final dust mass. The higher is the number of bursts (over the whole host galaxy evolution), the smaller is their intensity, approaching a 'quiescent-like' SFH (see model B5); the final dust mass is strongly limited by destruction (see Section 6.3.1).

This paper has been typeset from a TEX/LATEX file prepared by the author.